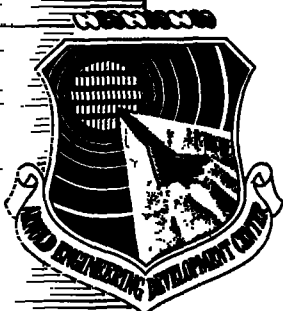


AEDC-TDR-63-93

C.1

DOC NUM SER CN
UNC11238-PDC A 1



ROCKET HEAT TRANSFER MEASURING DEVICES AND TECHNIQUES

*Compliments of the
AEDC Technical Library*

PROPERTY OF U. S. AIR FORCE
AEDC LIBRARY
AF 40(600)1000

By

**S. Wehofer
Rocket Test Facility
ARO, Inc.**

TECHNICAL DOCUMENTARY REPORT NO. AEDC-TDR-63-93

July 1963

AFSC Program Area 750G , Project 6950 , Task 695006

(Prepared under Contract No. AF 40(600)-1000 by ARO, Inc.,
contract operator of AEDC, Arnold Air Force Station, Tenn.)

ARNOLD ENGINEERING DEVELOPMENT CENTER

AIR FORCE SYSTEMS COMMAND

**UNITED STATES AIR FORCE
TECHNICAL REPORTS
FILE COPY**

NOTICES

Qualified requesters may obtain copies of this report from ASTIA. Orders will be expedited if placed through the librarian or other staff member designated to request and receive documents from ASTIA.

When Government drawings, specifications or other data are used for any purpose other than in connection with a definitely related Government procurement operation, the United States Government thereby incurs no responsibility nor any obligation whatsoever; and the fact that the Government may have formulated, furnished, or in any way supplied the said drawings, specifications, or other data, is not to be regarded by implication or otherwise as in any manner licensing the holder or any other person or corporation, or conveying any rights or permission to manufacture, use, or sell any patented invention that may in any way be related thereto.

ROCKET HEAT TRANSFER
MEASURING DEVICES AND TECHNIQUES

By

S. Wehofer

Rocket Test Facility

ARO, Inc.

a subsidiary of Sverdrup and Parcel, Inc.

July 1963

ARO Project No. RW2040

FOREWORD

The author acknowledges the efforts of Mr. O. C. Allen, who assisted in the data reduction program, and Mr. C. A. Neel, who supervised the programming and operation of the transient numerical equations for the IBM 7070 Digital Computer. Acknowledgement is also made to Mr. C. W. Bearden, for his assistance in conducting the experimental program.

ABSTRACT

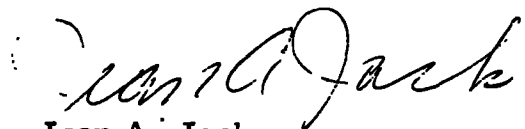
An investigation was conducted to find suitable devices and techniques for measuring heat transfer rates in the base areas of rocket-powered missiles. A slug mass calorimeter was selected to measure total (convective and radiant) heat rates, and a black-body cavity was selected to measure radiant heat rates. Similar instruments have been used in past test programs; however, the simplifying methods of analysis as used in the past with these instruments may result in considerable errors. The approach taken in this report was to determine the source heat rate by writing a general heat balance equation as a function of time about the heat sensing unit. An experimental program, utilizing a box-type muffle furnace to achieve a known source heat rate, was conducted to determine the accuracy of the mathematical analysis used herein. The results of the experimental program illustrated that heat transfer rates may be measured with reasonable accuracy providing basic fundamentals are adhered to and good engineering practices are utilized in the instrument design. In addition, the instruments and techniques as presented in this report should, in general, apply to other testing applications.

PUBLICATION REVIEW

This report has been reviewed and publication is approved.



Robert C. Harrison
Lt Col, USAF
AF Representative, RTF
DCS/Test



Jean A. Jack
Colonel, USAF
DCS/Test

CONTENTS

	<u>Page</u>
ABSTRACT	v
NOMENCLATURE	ix
1.0 INTRODUCTION	1
2.0 ANALYSIS OF SLUG MASS CALORIMETER	2
3.0 ANALYSIS OF BLACK-BODY CAVITY	9
4.0 EXPERIMENTAL PROGRAM	15
5.0 RESULTS AND DISCUSSION	18
6.0 CONCLUDING REMARKS	22
REFERENCES.	23

TABLES

1. Thermal Properties Used for the Experimental Program	25
2. Physical Constants Used for the Black-Body Cavity.	25

ILLUSTRATIONS

Figure

1. Slug Mass Calorimeter	27
2. Two-Dimensional Grid-Network for Calorimeter Insulation	28
3. Slug Mass Calorimeters	
a. Surface Heat Transfer Measurements	29
b. Surface and Back Heat Transfer Measurements	29
4. Black-Body Cavity.	30
5. External Flow Field over Cavity Aperture	31
6. Identification of Black-Body Cavity Parts	32
7. Black-Body Cavity (High Heat Rates).	33
8. Black-Body Cavity (Low Heat Rates).	34

<u>Figure</u>	<u>Page</u>
9. Experimental Black-Body Radiation Source	35
10. External Forced Convection Simulation Tube . . .	36
11. Experimental Slug Mass Calorimeter	37
12. Experimental Black-Body Cavity	38
13. Calorimeter Temperature-Time Histories	
a. $Q_{\text{source}} = 7.02 \text{ Btu/ft}^2\text{-sec}$	39
b. $Q_{\text{source}} = 13.55 \text{ Btu/ft}^2\text{-sec}$	40
14. Calorimeter Heat Rate-Time Histories	
a. $Q_{\text{source}} = 7.02 \text{ Btu/ft}^2\text{-sec}$	41
b. $Q_{\text{source}} = 13.55 \text{ Btu/ft}^2\text{-sec}$	42
15. Typical Temperature Distributions in the In- sulator Adjacent to the Calorimeter	
a. Side Temperature Distribution	43
b. Back Temperature Distribution	44
16. Black-Body Cavity Temperature-Time Histories	
a. 0.05-in. Aperture	45
b. 0.15-in. Aperture	46
17. Black-Body Cavity Heat Rate-Time Histories	
a. 0.05-in. Aperture (Time Zero at 3.75 sec)	47
b. 0.15-in. Aperture (Time Zero at 2.5 sec)	48
c. 0.15-in. Aperture (Time Zero at 1.25 sec)	49
18. Black-Body Cavity Temperature-Time Histories (External Convection)	
a. 0.05-in. Aperture	50
b. 0.15-in. Aperture	51
19. Black-Body Cavity Heat Rate-Time Histories (External Convection)	
a. 0.05-in. Aperture	52
b. 0.15-in. Aperture	53

NOMENCLATURE

A	Heat transfer area, ft^2
c_p	Specific heat, $\text{Btu/lb}_m\text{-deg}$
D	Diameter, ft
F	Angle factor
h	Film coefficient, $\text{Btu/ft}^2\text{-hr-deg}$
k	Thermal conductivity, $\text{Btu/ft}^2\text{-hr-deg/ft}$
l	Height of black-body cavity cone, ft
m	Mass, lb_m
Q	Heat transfer rate at any time, units as specified
r	Radius, ft
S	Internal surface area of the black-body cavity, ft^2
S_o	Equivalent surface area of a sphere of the same depth as the black-body in the normal direction of the aperture, ft^2
s	Cross-sectional area of the aperture, ft^2
T	Temperature, $^{\circ}\text{R}$
T'	Temperature after a small time increment, $^{\circ}\text{R}$
t	Thickness, ft
x, y	Distance, ft
α	Thermal diffusivity = $\frac{k}{\rho c_p}$, ft^2/hr
β	Time as used in Eq. (3), hr
δ	Increment of distance, ft
ϵ	Emissivity
ϵ_o	Apparent emissivity of a black-body
θ	Time, hr
λ	Integration variable (time)
ρ	Density, lb_m/ft^3
σ	Stephan-Boltzmann constant, 0.1713×10^{-8} $\text{Btu/ft}^2\text{-hr-}^{\circ}\text{R}^4$

ϕ	Surface temperature function
ψ	Half angle of black-body cone

SUBSCRIPTS

1, 2	Refer to location or component
A	Calorimeter
B	Insulator
C	Thermocouple
D	Heat sensor
G	Gas
i	Initial

1.0 INTRODUCTION

Attempts to measure heating rates during various simulated altitude tests of missile bases at AEDC and elsewhere have not been entirely successful, primarily because of inadequacies in heat transfer measuring equipment and techniques. The specific purpose of this program was to produce suitable devices and techniques for measuring heat transfer rates in the base area of rocket-powered missiles; however, the content of this report is not restricted to this application and may find use in other types of test programs, such as nose cones, re-entry bodies, and duct flow. This investigation was conducted in the Rocket Test Facility (RTF), Arnold Engineering Development Center (AEDC), Air Force Systems Command (AFSC).

The intent of a given test program will determine the specific parameters which are to be measured, and for the purpose of this report, it was assumed the following missile base parameters are desired: (1) convective heat rates, (2) radiant heat rates, and (3) base gas film coefficients. Film coefficients are particularly important if experimental data are to be presented in a general form to be useful in the formulation of theoretical analysis. Devices and methods of determining the above parameters are varied and numerous, but conditions which are associated with the measurement of heat rates on a missile base limits the selection of appropriate instrumentation. These limitations dictate that:

1. The instruments must be of a flight-weight type and robust to survive rough handling and the intense vibrations which are associated with the start transients of rockets,
2. The instruments must not be adversely affected by deposition of combustion exhaust products on their surfaces,
3. The instrument used to measure convective heat rates must not appreciably disturb the thermal characteristics of the base, and
4. The instruments should be designed so they are amenable to mathematical analysis.

To measure the total heat rate, an insulated slug mass was selected which had approximately the thickness and was constructed of the same material as the base. For short duration tests, it is necessary to duplicate

Manuscript received April 1963.

only the depth of the material which will be affected by a thermal change during the test. To measure radiative heat rates, a black-body cavity similar in concept to the cavity utilized by various organizations as a radiative standard (Refs. 1 and 2) is proposed. Upon determining total and radiant heat rates, the gas film coefficient may be evaluated by measuring the base gas temperature. No analysis is presented concerning gas temperature measurements since several adequate probes of this nature have already been developed and analyzed (see Refs. 3, 4, and 5).

Similar instrumentation to that proposed herein has been used on past test programs. The general method of analysis, however, was to assume that the change of internal energy of the heat sensing unit was equal to the source heat rate or to compare experimental results with laboratory calibrations to determine the source heat rate. It was shown during this investigation that both these methods may be greatly in error. The approach utilized in this report was to determine the source heat rate by writing a general heat balance equation as a function of time about the heat sensing unit. Because it was impractical to try to anticipate every type configuration and the appropriate method of mathematical evaluation, a design was selected which, in general, would apply to heat transfer measurements encountered in rocket base heating tests. However, it should be stressed that each system should be analyzed on its own merits to determine what, if any, valid simplifying assumptions may be made to assist in the reduction of the data.

2.0 ANALYSIS OF SLUG MASS CALORIMETER

In the earlier phases of this program, Westkaemper (Ref. 6) analyzed the factors influencing accuracy when using a slug mass calorimeter to determine total source heat rates. The principal conclusions in Ref. 6 are:

1. The effects of surface temperature mis-match between the measuring device and surrounding base is a source for considerable error. The magnitude of this error (as stated in Ref. 6) has since been found to be somewhat pessimistic (Ref. 7); however, a temperature mis-match is still a large potential source of error.
2. The calorimeter should duplicate the surface conditions of the segment it replaces.
3. The calorimeter mounting insulation may be a source of considerable conduction losses.

Adherence to the first and second conclusions is particularly important on multi-jet missile bases, since at present no adequate theory exists to predict the magnitude of the effect caused by deviation from actual base similarity (change of base thermal characteristics). It is generally not possible to have complete similarity and, in fact, it may be desirable to accept a negligible or known deviation in dimensional similarity which will simplify the mathematical analysis; however, because of the present state-of-the-art of determining missile base flow fields, any deviations should be meticulously analyzed. For instance, a common practice in rocket measuring techniques is to calibrate a slug-mass calorimeter with a radiant heat source and compare experimental temperature histories to the laboratory calibration results and determine the experimental source total heat rate. For this method to be successful, either the surrounding environment of the calorimeter would have to be controlled to that of the laboratory calibration or the calorimeter encased in a quantity of insulation which would isolate the unit from its surrounding environment. The above methods, to control or isolate the surrounding environment, could have a strong effect on the gas film coefficient and, hence, on the measured source heat rate. Also, when calibrating with a radiant heat source, the heat rate absorbed is a direct function of the calorimeter absorptivity which, in general, is a very sensitive parameter.

2.1 MATHEMATICAL MODEL

A schematic of the calorimeter which is to be analyzed is shown in Fig. 1. The following conditions and assumptions are specified:

1. The calorimeter is made of the same material with approximately the same thickness and has the same surface conditions and contour as the segment of the base which it replaces.
2. The thermocouple leads are infinitely long and perfectly insulated.
3. Thermal contact resistances at interfaces between materials are zero.
4. The surface emissivity and absorptivity of the calorimeter are known and equal.
5. The calorimeter and the base are respectively Newtonian (negligible internal thermal resistance).
6. Thermal properties for all the constituents are independent of temperature.
7. The thickness of the insulation is small compared to the radius of the calorimeter.

8. The heat rate is uniform over the surface of the calorimeter but may vary with time.
9. The temperature-time history for the calorimeter may be expressed, for mathematical convenience, by an empirical equation of the following form:

$$T_A (\theta) = T_i + B (1 - e^{-Z \theta}) \quad (1)$$

where

B = experimental constant, °R

Z = experimental constant, per hr

All data from base heating tests encountered thus far were found to fit the above relation; however, any other suitable relation may be used.

For any given time, the following heat balance may be written about the calorimeter:

$$Q_{A_{Total}} = Q_{A1} + Q_{A2} + Q_{A3} + Q_{A4} \quad (2)$$

where

$Q_{A_{Total}}$ = total heat rate to the calorimeter

Q_{A1} = change of internal energy in the calorimeter

Q_{A2} = conduction losses through the thermocouple leads

Q_{A3} = conduction losses into the insulator

Q_{A4} = re-radiation losses from the calorimeter

Furthermore (Refer to Fig. 2 for the location of the x and y axes):

$$Q_{A_{Total}} = A_A h_C \left\{ T_G (\theta) - [B (1 - e^{-Z \theta}) + T_i] \right\} + \epsilon_A A_A Q_{G_{Radiation}} \quad (2a)$$

$$Q_{A1} = m_A c_{p_A} (B Z e^{-Z \theta}) \quad (2b)$$

$$Q_{A2} = -k_C \pi r_C^2 \left. \frac{dT_A (\theta)}{dx_C} \right|_{x_C=0} \quad (2c)$$

$$Q_{A3} = - \frac{k_B \pi D_A}{\delta_2} \int_0^{t_A} [T_B (x, y, \theta) - T_A (\theta)]_{y=\delta_2} dx - \frac{2 k_B \pi}{\delta_1} \quad (2d)$$

$$\int_0^{t_A} y [T_B (x, y, \theta) - T_A (\theta)]_{x=\delta_1} dy$$

$$Q_{A4} = \epsilon_A A_A \sigma [B (1 - e^{-Z \theta}) + T_i]^4 \quad (2e)$$

2.2 SOLUTION OF THERMOCOUPLE LOSSES

Reference 8 presents the following approximate solution for one-dimensional heat flow in a semi-infinite slab with a uniform initial temperature:

$$\left. \frac{dT}{dx} \right|_{x=0} \approx \sqrt{\frac{1}{a\pi}} \left[2\beta^{1/2} \phi'(\theta) + \frac{\phi(\theta-\beta)}{\beta^{1/2}} \int_0^{\theta-\beta} \frac{\phi(\lambda)}{2(\theta-\lambda)^{3/2}} d\lambda \right] \quad (3)$$

for $\beta > 0$

From Eq. (1):

$$\phi(\theta) = B(1 - e^{-Z\theta})$$

$$\phi(\theta-\beta) = B[1 - e^{-Z(\theta-\beta)}]$$

and letting $\mu = \theta - \lambda$

$$\phi(\lambda) = \phi(\theta - \mu) = B[1 - e^{-Z(\theta-\mu)}]$$

Now substituting the above relations into Eq. (3) and integrating and substituting the result into Eq. (2c), the following solution is obtained:

$$\begin{aligned} Q_{A2} \approx \frac{k_C r_C^2}{\sqrt{a_C/\pi}} & \left\{ 2BZ\beta^{1/2} e^{-Z\theta} + \frac{B[1 - e^{-Z(\theta-\beta)}]}{\beta^{1/2}} + \frac{B}{\theta^{1/2}} - \frac{B}{\beta^{1/2}} \right. \\ & - B e^{-Z(\theta-\beta)} \left[-\frac{1}{\beta^{1/2}} + 2Z\beta^{1/2} - \frac{4}{3}Z^2\beta^{3/2} + \frac{8}{15}Z^3\beta^{5/2} - \dots \right] \\ & \left. + B \left[-\frac{1}{\theta^{1/2}} + 2Z\theta^{1/2} - \frac{4}{3}Z^2\theta^{3/2} + \frac{8}{15}Z^3\theta^{5/2} - \dots \right] \right\} \quad (4) \end{aligned}$$

for $\beta > 0, Z > 1; \theta < 1$

2.3 SOLUTION OF INSULATOR LOSSES

In order to solve Eq. (2d), a two-dimensional grid-network was constructed (Fig. 2) and solved by explicit numerical methods. Only the generalities of this system are discussed because a thorough explanation is presented in Ref. 9 and also some discussion is presented in Ref. 6. The total number of grid points to be used will have to be a compromise between the type data reduction program and the particular application compared to the degree of accuracy required. One simple means to size the

network is to apply a given set of data and increase the network and compare the deviations of the results, or the analytical method in Ref. 10 may be used to estimate the truncation error. Having the experimental temperature-time histories for the boundaries of the insulator, the grid-network may be solved to determine the temperature gradient in the insulator adjacent to the calorimeter. A typical calculation for the inner portion of the insulator (see Fig. 2) is

$$\frac{2}{MN} (T_1' - T_1) = M (T_1 - T_1) + M (T_{10} - T_1) + \frac{1}{M} (T_1 - T_1) + \frac{1}{M} (T_{11} - T_1)$$

where

$$M = \frac{\delta_1}{\delta_2}$$

$$N = \frac{1}{1 + M^2} = \frac{2 \Delta \theta k_B}{c_{p_B} \rho_B \delta_1^2} = \frac{2 \Delta \theta \alpha_B}{\delta_1^2}$$

A typical calculation for the surface of the insulator is

$$\frac{k_B}{MN} (T_1' - T_1) = Q_{B_{Total}} + \frac{k_B M}{2} (T_2 - T_1) + \frac{k_B M}{2} (T_4 - T_1) + \frac{k_B (T_2 - T_1)}{M}$$

where

$$Q_{B_{Total}} = \delta_2 h_G [T_G(\theta) - T_1] + \epsilon_B \delta_2 Q_{B_{Radiation Interchange}}$$

Since the solution of the grid-network includes $Q_{B_{Total}}$, another assumption is required. If the gas film coefficient for the insulator and the calorimeter are assumed to be equal and if the base gas temperature history is known, the preceding equations may be solved by an iterative method. This procedure can prove to be quite awkward; however, if the calorimeter configuration is changed as shown in Fig. 3a, the analytic solution will be greatly simplified. In analyzing this configuration, the assumptions and conditions are the same as previously stated with the addition that the lateral heat conduction from the base through the interconnecting strip of metal to the calorimeter is negligible. This configuration has two principal advantages:

1. Since the temperature history is known for all the boundaries of the insulator, a solution may be obtained directly without resorting to iteration procedures, and
2. The interconnecting strip of metal will duplicate the surface conditions and if it is relatively short it should remain in temperature equilibrium with the calorimeter and eliminate large surface temperature gradients.

2.4 VARIATION OF THERMAL PROPERTIES WITH TEMPERATURE

If a large temperature rise is encountered by the calorimeter, the assumption of constant thermal properties for the insulator will probably not be valid. Since the insulator should be relatively thin and since there is no special need for the insulator to have a particularly low thermal diffusivity, the thermal diffusivity of the insulator may be estimated at the temperature level of the calorimeter or the average temperature of the calorimeter and adjacent base, whichever is more representative of the temperature level in the insulator. If the thermal properties of the insulator are estimated at the temperature of the calorimeter, the equations for the grid-network would be affected as follows:

$$\alpha_B (T_A) = \frac{k_B (T_A)}{\rho_B (T_A) c_{pB} (T_A)}$$

$$\Delta \theta = \frac{\delta_i^2}{2 \alpha_B (T_A)} \frac{1}{1 + M^2}$$

$$N = \frac{2 \Delta \theta \alpha_B (T_A)}{\delta^2}$$

The variation of the thermal diffusivity as a function of the calorimeter temperature will depend upon the particular insulating material. Care should be exercised in the above relations to ensure that the time increment does not become infinitesimally small or excessively large because of computation time and truncation error, respectively.

2.5 CALORIMETER TEMPERATURE GRADIENTS

It may not always be possible to adhere to the assumption of a Newtonian calorimeter; however, the calorimeter should be sized so that only temperature variation along one axis need be considered. One simple means of determining the severity of the temperature gradient is to assume that the calorimeter is a semi-infinite solid with a constant heat rate. Reference 11 presents the following relation for the temperature distributions of this case as a function of time and distance:

$$T_A (x, \theta) = T_{Ai} + \frac{Q_{source}}{k_A} \left[2 \sqrt{\frac{\alpha_A \theta}{\pi}} e^{-x^2/4 \alpha_A \theta} - x \operatorname{erfc} \frac{x}{2 \sqrt{\alpha_A \theta}} \right] \quad (5)$$

Now for any given time (θ), the above equation can be solved for x equal zero and x equal to the thickness of the calorimeter, and the resulting temperature difference can be analyzed. It must be remembered that the above is a very pessimistic result because, for the application in this

report, the calorimeter cannot be considered as a semi-infinite solid. If the calorimeter cannot be considered Newtonian, there are several means by which the effect of the temperature gradient may be compensated.

1. Construct a grid network similar to the one used for the insulator.
2. Measure the surface and rear face temperature of the calorimeter and assume a linear relation between these two points. An equation of the following type is obtained:

$$T_A(x_A, \theta) = T(\theta)_1 - \left[\frac{T(\theta)_1 - T(\theta)_2}{t_A} \right] x_A$$

where

$T(\theta)_1$ is the surface temperature history

$T(\theta)_2$ is the back face temperature history

3. Embed the measuring thermocouple at the center of the calorimeter and assume the resulting temperature history is the average temperature between the front and back surface. When embedding a thermocouple within the calorimeter, a calculated estimate should be made of the error caused by the disturbance of the calorimeter temperature field from the thermocouple insert.

2.6 HEATING OF THE BACK SURFACE

In some instances, a base configuration may be encountered for which it is necessary to determine the net heating rate from both sides of the base, such as a protective flame shield where afterburning of fuel-rich exhaust products may occur on the back side. A calorimeter configuration as shown in Fig. 3b may be utilized; however, the gas film coefficients cannot be determined for this particular design. If this information is desired, two calorimeters as shown in Fig. 3a, inverted with respect to each other, should be used.

2.7 SURFACE CONTAMINATION

One problem encountered with the use of the calorimeter is the determination of any change in surface emissivity which may be caused by rocket exhaust product contamination. One method which has been attempted on past missile base heating test programs was to use a polished calorimeter (absorptivity near zero) and a blackened calorimeter (absorptivity near unity) and to assume that the difference between the

indicated heat rate of each calorimeter is equal to the source radiant heat rate. Because of contamination and high base gas temperatures, it is virtually impossible to maintain the highly reflective calorimeter surface. Fortunately, the indication to date is that the radiant heat flux is generally much less than the convective heat fluxes for most missile bases. Furthermore, the measuring devices proposed in this report will allow the radiant heat rate to be measured separately from the total heat rate, and this will assist in the analysis of the contamination problem as it affects the slug mass calorimeter.

3.0 ANALYSIS OF BLACK-BODY CAVITY

A schematic of the instrument selected to measure radiant heat rates is shown in Fig. 4. A similar device is reported in Ref. 12. The principal difference is that the instrument used in Ref. 12 has a lens between the aperture and heat sensing unit in conjunction with an internal passage through which air is bled to prevent contamination of the lens. In addition, the instrument in Ref. 12 is not particularly amenable to mathematical analysis but rather relies upon interpolation of experimental data obtained from a laboratory calibration. This makes it necessary to maintain the external environment of the heat sensor similar to that for the calibration. Although the use of a lens is advantageous in that the heat sensing unit is isolated from external convection currents, the other requirements (air jet and controlled environment) make this instrument impractical for flight test missiles. The device used in this investigation has an open aperture through which the radiant heat is transmitted. The sizing of the aperture to prevent external convective currents from strongly influencing the cavity temperature history is a problem of an extremely complex nature (see Fig. 5 for a pictorial illustration of this effect); therefore, this phenomenon was investigated experimentally.

3.1 MATHEMATICAL MODEL

In analyzing the configuration in Fig. 4, the following conditions and assumptions are specified:

1. All metal parts are Newtonian.
2. The thermocouple leads are infinitely long and perfectly insulated.
3. Thermal contact resistances at interfaces are zero.
4. The emissivity of the cavity is equal to the absorptivity.
5. Convective heating within the cavity is negligible.

6. The reflections of radiant energy within the cavity are diffused.
7. The influence of the metal cap on the temperature gradient in the insulator behind the heat sensor is negligible.
8. All of the incident incoming radiation on the sides of the aperture walls is specularly reflected ($\alpha \ll 1$) and no energy is absorbed. This further implies that the angle factor from station 1 to station 2 (see Fig. 6) is unity.
9. The absorptivity for the surface of the heat sensor and the back surface of the metal cap is near unity.
10. The insulating washer which separates the metal cap and heat sensor has negligible effect on angle factors with respect to the heat sensor.
11. The temperature-time history for the heat sensor may be expressed by the following empirical relation:

$$T_D(\theta) = T_i + B' (1 - e^{-Z'\theta}) \quad (6)$$

where

B' = experimental constant, °R

Z' = experimental constant, per hr

12. The temperature-time history of the metal cap may be expressed by the following empirical relation:

$$T(\theta) = T_i + C' (1 - e^{-E'\theta}) \quad (7)$$

where

C' = experimental constant, °R

E' = experimental constant, per hr

For any given time, the following heat balance may be written about the heat sensor (refer to Fig. 6):

$$Q_D(1 \rightarrow 5) + Q_D(4 \rightarrow 5) = Q_{D1} + Q_{D2} + Q_{D3} + Q_{D4} \quad (8)$$

where

$Q_D(1 \rightarrow 5)$ = radiation through the aperture to the heat sensor

$Q_D(4 \rightarrow 5)$ = re-radiation from the base of the metal cap to the heat sensor

Q_{D1} = change in internal energy for the heat sensor

Q_{D2} = conduction losses through the thermocouple leads

Q_{D3} = conduction losses into the insulation

Q_{D4} = re-radiation from the heat sensor

Furthermore,

$$Q_D (1 \rightarrow 5) = \epsilon_0 A_D F_{1-s} \sigma T_s(\theta)^4 \quad (8a)$$

where

$$\epsilon_0 = \frac{\epsilon_D}{\epsilon_D (1 - s/S) + s/S} \left[1 + (1 - \epsilon_D) (s/S - s/S_0) \right] \quad (\text{Ref. 13})$$

$$F_{1-s} = 1$$

$T_s(\theta)$ = apparent radiant source black-body temperature

$$Q_D (4 \rightarrow 5) = \epsilon_4 A_4 F_{4-s} \sigma \left[C' (1 - e^{-E'\theta}) + T_i \right]^4 \quad (8b)$$

where

$$F_{4-s} = 1$$

$$Q_{D4} = \epsilon_D A_D F_D \sigma \left[B' (1 - e^{-Z'\theta}) + T_i \right]^4 \quad (8c)$$

where

$$F_D = \sin \psi \quad (\text{Ref. 14})$$

$$Q_{D1} = m_D c_{pD} B' Z' e^{-Z'\theta} \quad (8d)$$

$$Q_{D2} = -k_C \pi r_C^2 \left. \frac{dT_D(\theta)}{dx'_C} \right|_{x'_C = 0} \quad (8e)$$

$$Q_{D3} = -k_B \pi r_1 \sqrt{r_1^2 + \ell^2} \left. \frac{dT_D(\theta)}{dx'_B} \right|_{x'_B = 0} \quad (8f)$$

3.2 SOLUTION OF THERMOCOUPLE LOSSES

Equation (8e) can be solved by using Eq. (3), and the resulting equation is

$$Q_{D2} \approx \frac{k_C r_C^2}{\sqrt{a_c/\pi}} \left\{ 2B'Z'\beta^{1/2} e^{-Z'\theta} + \frac{B'[1 - e^{-Z'(\theta-\beta)}]}{\beta^{1/2}} - \frac{B'}{\beta^{1/2}} + \frac{B'}{\theta^{1/2}} \right. \\ \left. - B' e^{-Z'(\theta-\beta)} \left[-\frac{1}{\beta^{1/2}} + 2Z'\beta^{1/2} - \frac{4}{3}Z'^2\beta^{3/2} + \frac{8}{15}Z'^3\beta^{5/2} - \dots \right] \right. \\ \left. + B' \left[-\frac{1}{\theta^{1/2}} + 2Z'\theta^{1/2} - \frac{4}{3}Z'^2\theta^{3/2} + \frac{8}{15}Z'^3\theta^{5/2} - \dots \right] \right\} \quad (9)$$

for $\beta > 0, Z' > 1, \theta < 1$

3.3 SOLUTION OF INSULATOR LOSSES

If the insulation can be considered as a one-dimensional semi-infinite slab with a uniform initial temperature, Eq. (8f) may also be solved by Eq. (3), and the resulting equation is

$$Q_{D3} \approx \frac{k_B r_1 \sqrt{r_1^2 + l^2}}{\sqrt{a_c/\pi}} \left\{ 2B'Z'\beta^{1/2} e^{-Z'\theta} + \frac{B'[1 - e^{-Z'(\theta-\beta)}]}{\beta^{1/2}} - \frac{B'}{\beta^{1/2}} + \frac{B'}{\theta^{1/2}} \right. \\ \left. - B' e^{-Z'(\theta-\beta)} \left[-\frac{1}{\beta^{1/2}} + 2Z'\beta^{1/2} - \frac{4}{3}Z'^2\beta^{3/2} + \frac{8}{15}Z'^3\beta^{5/2} - \dots \right] \right. \\ \left. + B' \left[-\frac{1}{\theta^{1/2}} + 2Z'\theta^{1/2} - \frac{4}{3}Z'^2\theta^{3/2} + \frac{8}{15}Z'^3\theta^{5/2} - \dots \right] \right\} \quad (10)$$

for $\beta > 0, Z' > 1, \theta < 1$

To determine the amount of insulation which is required to satisfy Eq. (10), the following equations which are presented in Ref. 11 may be used.

Boundary conditions for the heat sensor are

$$T_B = T_i \text{ at } \theta = 0, x'_B \geq 0$$

$$T_B = T_i + B'(1 - e^{-Z'\theta}) \text{ at } x'_B = 0, \theta > 0$$

$$T_B = T_i \text{ at } x'_B = \infty, \theta \geq 0$$

The solution is

$$T_B(\theta, x'_B) = T_i + B^i \operatorname{erfc} X_B + \frac{B^i e^{-Z'\theta}}{2} \left\{ e^{-x'_B i \sqrt{Z'/a_B}} \operatorname{erfc} X_{B0} + e^{x'_B i \sqrt{Z'/a_B}} \operatorname{erfc} X_{B1} \right\} \quad (11)$$

where

$$X_B = \frac{x'_B}{2 \sqrt{a_B \theta}}$$

$$X_{B0} = X_B - i \sqrt{Z'\theta}$$

$$X_{B1} = X_B + i \sqrt{Z'\theta}$$

The same equation may be used for the external casing. Tables for the solution of probability integrals for complex argument are presented in Ref. 15. Now using Eq. (11), a temperature history for the heat sensor and external casing may be assumed, and the depth of penetration for an allowable temperature rise for any given time determined.

3.4 HIGH RADIANT HEAT RATE VALUES

For relatively high radiant heat rates, it is not desirable to isolate the heat sensor from the external casing because the large temperature gradient in the insulator will void the use of constant thermal properties when the heat losses into the insulator are calculated. Although the insulator losses may be calculated by determining the thermal properties as a function of the temperature level at given depths in the insulation, it is felt that the instrument shown in Fig. 7 will simplify this procedure. The insulation losses for this instrument are determined by using a two-dimensional grid-network (as previously discussed in section 2.3) with the thermal diffusivity of the insulator determined at the temperature level of the heat sensor or by using the average temperature between the heat sensor and external casing, whichever is more representative of the temperature level in the insulation. It may not always be possible to assume that the external casing is Newtonian, but this situation can be handled in the same manner as previously discussed for non-Newtonian slug mass calorimeters.

3.5 LOW RADIANT HEAT RATE VALUES

Since the ratio of the surface area of the heat sensor to the aperture area is relatively large for the black-body cavities considered, radiant

heat fluxes less than approximately 3 Btu/ft²-sec will be difficult to determine accurately because of the small temperature rise of the heat sensor. Fortunately, for the purpose of base heating tests, heat fluxes of this magnitude are insignificant and can generally be ignored. In other type testing applications it may be desirable to measure these values. The black-body configuration shown in Fig. 8 is analyzed as a means of measuring the lesser rates of radiant heat fluxes. The principal advantage of this instrument is that the air-gap between the heat sensor and backing plate may be evacuated, and the conduction losses from the back of the heat sensor are greatly reduced. The conditions and assumptions for this design are the same as previously stated for the other black-body cavity with the following additions:

1. The pressure in the evacuated region between the heat sensor and the backing plate is maintained in a rarefied regime so that thermal conductance in this region is negligible.
2. The angle factor between the heat sensor and backing plate may be determined by considering the two bodies as infinite parallel planes each at uniform temperature at any time (θ)
3. The temperature history for the heat sensor and backing plate may be expressed by the same type exponential equation as previously used for the heat sensor.

Now the following heat balance may be written about the heat sensor (refer to Fig. 6):

$$Q_D (1 \rightarrow 5) + Q_D (4 \rightarrow 5) = Q_{D_1} + Q_{D_2} + Q_{D_4} + Q_D (5 \rightleftharpoons 6) \quad (12)$$

where

$Q_D (5 \rightleftharpoons 6)$ = radiation interchange between the heat sensor and the backing plate

also

$$Q_D (5 \rightleftharpoons 6) = \frac{A_D \sigma}{1/\epsilon_D - 1/\epsilon_6 - 1} [T_D(\theta)^4 - T_6(\theta)^4] \quad (13)$$

where

$T_D(\theta)$ = temperature heating for the heat sensor

$T_6(\theta)$ = temperature history for the backing plate

The other terms in Eq. (12) are the same as those used in Eq. (8). It should be noted that, for low emissivity values for the back of the heat sensor and the face of the backing plate, the corresponding temperature rise for the heat sensor at a given source heat rate is much greater. Therefore, polished surfaces are desirable because the equation which will express the temperature history of the heat sensor can be more accurately defined.

3.6 MEASUREMENTS IN SPECIFIC AREAS

One advantage to the use of an aperture is that it may be sized to measure radiant heat rates from specific areas in the base region if the side walls of the aperture are made of a non-reflecting material (absorptivity is unity) so that only the direct radiation will enter the cavity.

The angle factor for direct radiation is (refer to Fig. 6)

$$F_{1-2} = 1 + 2 \left(\frac{x}{D} \right)^2 - 2 \frac{x}{D} \sqrt{(x/D)^2 + 1} \quad (\text{Ref. 16}) \quad (14)$$

Therefore, by properly sizing the x/D ratio for the aperture, the field of view for the cavity can be controlled. In blackening the aperture walls, the re-radiation from the walls of the aperture to the heat sensor may become significant, and this may be accounted for as follows (refer to Fig. 6)

$$Q_D (3 \rightarrow 5) = \epsilon_s A_s F_{3-s} \sigma \left[T_i + C' (1 - e^{-E' \theta}) \right]^4 \quad (15)$$

where

$$F_{3-s} = 1/4 \left[\sqrt{(x/D)^2 + 4} - x/D \right] \quad (\text{Ref. 14})$$

4.0 EXPERIMENTAL PROGRAM

4.1 CALIBRATION FURNACE

To determine the effectiveness of the general mathematical procedures as used in this report, a series of bench calibrations was conducted with a black-body radiant energy source. The particular design used for the black-body was adapted from the one described in Ref. 17 and illustrated in Fig. 9. The inner liner which simulates the black-body is graphite ($\epsilon \approx 0.95$), and by using the following equation

$$\epsilon_o = \frac{\epsilon_{gr}}{\epsilon_{gr} (1 - s/S) + s/S} \left[1 + (1 - \epsilon_{gr}) (s'/S - s/S_o) \right] \quad (16)$$

where

ϵ_{gr} = emissivity of the graphite

the emissivity of the liner aperture is calculated to be greater than 0.99. A description of the furnace used for the calibrations is as follows:

Heating elements - molybdenum
Insulation - firebrick

Maximum operating temperature	- 3560°R
Maximum temperature variation within the center section	- ± 4 deg
Inert atmosphere	- helium
Helium flow rate	- approximately 80 scfh

The temperature of the furnace was automatically controlled by a photo-electric cell which was sighted on the furnace wall. The temperature of the graphite liner was measured with a planinum-platinum-rhodium thermocouple monitored on a sixteen-point recorder and also with an optical pyrometer. The calibration of the pyrometer was compared to a National Bureau of Standards calibrated tungsten filament. All other temperatures were recorded on an eighteen-channel oscillograph. The uncertainty of the source heat rate calculated from the furnace temperature measurements is estimated to be five percent.

To determine the magnitude of the thermal effect of external forced convection on the black-body cavity, an inconel tube was inserted into the graphite liner to permit flowing of helium gas over the surface of the instrument (Fig. 10). The intent of this investigation was not to bracket the phenomenon completely but only to determine the strength of this effect for external velocities which were felt to be representative of the upper values encountered on missile bases and for cavity apertures not exceeding 0.15 in. Because of uncertainty in the exact temperature rise of the helium gas as it passed through the inconel tube, the exit velocity of the gas from the tube was conservatively estimated, based on the volume flow and pressure measurement of the gas, to be 1500 ft/sec. The leakage rate of the graphite liner and furnace was great enough so that for steady-state conditions the liner was not pressurized.

4.2 SLUG MASS CALORIMETER

The slug mass calorimeter used for the program is illustrated in Fig. 11. Iron-constantan thermocouples (28 gage) were spot welded to the slug mass and to the side and back of the metal casing. The insulating material was a polytrifluorochloroethylene plastic. The calorimeters were stainless steel type 347, and each was weighed and measured prior to installation. The metal casings for each instrument had a 45-deg lip to ensure that the surface of the calorimeter was flush with the inside of the graphite liner and had a rod attached to the rear of the casing to enable insertion into the liner aperture. Information was available for the emissivity of the calorimeter ($\epsilon = 0.39$ for $T < 860^\circ\text{R}$, Ref. 18). The

surface emissivity of the insulator was unknown, therefore, the insulator was coated with a rough layer of lamp black ($\epsilon = 0.8$, Ref. 18).

4.3 BLACK-BODY CAVITY

A schematic of the black-body cavity which was calibrated is shown in Fig. 12. The entire internal surface of the cavity was coated with a commercial optical black paint, while the side walls of the aperture were polished. Iron-constantan thermocouples (28 gage) were spot welded to the copper heat sensor and the stainless steel surface cap. The insulating material was polytrifluorochloroethylene plastic. Each of the copper cones was weighed and measured prior to installation. The aperture sizes which were used for this program were:

<u>Aperture Diameter, in.</u>	<u>Aperture D/λ</u>
0.05	1.67
0.15	5.00

All of the thermal properties and physical dimensions used in this report are presented in Tables 1 and 2 and Figs. 13 through 19.

4.4 PROCEDURE

1. The desired furnace temperature was set with the automatic control system, and after obtaining the pre-set temperatures the furnace was allowed to soak for an additional hour to ensure temperature uniformity.
2. After the soaking period had been completed, the optical pyrometer was sighted through the front of the furnace in order to determine accurately the graphite liner temperature.
3. The flow of the inerting atmosphere was reduced to less than 10 scfh.
4. The enclosure over the front of the aperture in the furnace door was removed and the instrument inserted into the graphite liner aperture. The time required to seat the instrument was on the order of one second. When the instrument was seated, a blip on the oscillograph trace indicated time zero.
5. When determining the thermal effect of external forced convection on the black-body cavity, the same procedure as described above was followed with the addition that when the instrument was seated in the graphite liner an off-on hand valve in the external flow simulation tube was opened.

5.0 RESULTS AND DISCUSSION

5.1 SLUG MASS CALORIMETER

Two typical experimental temperature-time histories for the calorimeter along with the respective boundary temperature histories are illustrated in Figs. 13a and b with the corresponding exponential equation presented with each curve. In fitting the exponential equation to the experimental temperature-time curve, the deviation was never more than a few degrees; therefore, only the experimental curve was presented. The respective corrected heat rate-time histories are presented in Figs. 14a and b. Change in internal energy, re-radiation, and thermocouple losses were calculated as outlined in section 2.1. An emissivity value of 0.4 was used in determining the radiation losses from the calorimeter surface. It was first considered that the calorimeter emissivity might change significantly when exposed to the furnace temperature; however, it was found that no significant change occurred in the temperature-time history of the calorimeter when it was used twice to measure the same source heat rate. The fact that there was no apparent change in the calorimeter surface emissivity is attributed to the inerting helium atmosphere and the short exposure time. Also, each calorimeter was used only a limited number of times. Equation (4), which is used to determine the heat loss into the thermocouple leads, was programmed on a 7070 IBM digital computer and the series which is part of this equation was expanded to include twenty terms. In determining the losses and gains from and into the insulation, a grid-network 45 units in depth and 50 units in width was used. The heat balance equations for the grid-network were also programmed on the 7070 IBM digital computer, and the temperature field in the insulation for specified time periods was obtained as the end result. The grid network was solved in the same manner as previously discussed except $Q_{B_{Total}}$ for this instance was:

$$Q_{B_{Total}} = \epsilon_B \delta_2 \sigma (T_f'^4 - T_s'^4)$$

where

T_f = graphite liner temperature, °R

T_s' = surface grid temperature after time $\Delta\theta$, °R

The temperature of the surface grids was calculated by iterating the individual grid heat balance until the temperature determined from the incoming radiant heat rate was equal to the corresponding temperature for the heat balance at the particular time increment. The tabulated temperatures from the digital computer were plotted graphically versus position with respect to the calorimeter. Figures 15a and b show two typical temperature distributions in the insulator adjacent to the side and rear,

respectively, of the calorimeter. The net exchange of heat between the calorimeter and insulator was determined by using a planimeter to measure the area between the calorimeter temperature curve and the temperature distribution in the insulator next to the calorimeter. In retrospect, because of the upper temperature limit of fluoro-carbon plastics, a ceramic-type material would have served more favorably as the insulating material; however, in consideration of the relatively short time periods involved, no significant adverse effects were noticeable. In addition, the thermal characteristics of this material made it possible to approximate constant values for the thermal conductivity and specific heat at the average temperature of the calorimeter.

With reference to Figs. 14a and b, the curvature of the calculated source heat rate is the effect of using constant thermal properties for the insulator in the calculation of the grid-network. This curvature will become more pronounced as the source heat rate increases, and, in actual testing applications the change of thermal properties with temperature must be considered. The important factor, therefore, in selecting an insulating material for use with the calorimeter is that it have known thermal properties as a function of temperature. Reference 19 presents the thermo-physical properties as a function of temperature for numerous insulating materials. Figures 14a and b also illustrate that for even a good insulation material the conduction losses into the insulator can be quite significant. In fact, the calorimeters used in base heating tests will, in all probability, be thicker and exposed to heating rates greater than the values encountered. These factors will further increase the error in assuming that the source heat rate is equal to the change in internal energy of the calorimeter.

The results of the mathematical computations illustrate that total source heat rates can be calculated with reasonable accuracies if a complete heat balance is written about the calorimeter. Also, the accuracy in determining source heat rates should improve as the source heat rate increases because a small error in the measurement of the temperature or in curve fitting will have a less pronounced effect on the results.

5.2 BLACK-BODY CAVITY

Two typical temperature-time curves for the black-body cavity without external flow are presented in Figs. 16a and b. The empirical equation used for the purpose of calculations is presented with each curve. The respective heat rate-time histories are shown in Figs. 17a and b. The change in internal energy and re-radiation gains and losses were calculated as outlined in section 3.1. An emissivity value of unity was used in determining the radiation from the heat sensor and surface cap. The radiation

interchange with the sides of the aperture wall was assumed to be negligible. The thermocouple and insulator losses for the experimental curve in Fig. 16b were calculated from Eqs. (9) and (10), respectively. In determining the thermocouple and insulator losses for the experimental curve in Fig. 16a the following equation was used:

$$Q = \frac{2kA\bar{C}\theta^{1/2}}{\sqrt{\pi a}} \quad (17)$$

where

\bar{C} is the temperature-time slope
of the experimental curve, deg/hr

Equation (17) is the solution of the one-dimensional heat conduction equation of a semi-infinite slab with a uniform initial temperature where the surface temperature history is a linear relation with time. The initial thermal lag of the heat sensing unit (Figs. 16a and b) is attributed to the magnitude of the heat sensor surface area compared to the magnitude of the heat rate encountered and to the location of the thermocouple leads at the apex of the cone. Therefore, in calculating the change in internal energy, insulator losses, and thermocouple losses, time zero was considered as the point in the initial portion of the temperature-time history where an inflection occurred in the slope of the curve. In Figs. 16a and b the inflection was considered to be at 3.75 and 2.5 sec, respectively. This inflection point may be difficult to determine accurately, particularly for low magnitudes of radiant heat rates. The source heat rate was calculated for the temperature curve in Fig. 16b assuming that the inflection point occurred at 1.25 sec rather than 2.5 sec. The temperature-time relation then becomes

$$T_A(\theta) = 205(1 - e^{-78\theta}) + 541.5$$

and the heat rate-time history using this expression is shown in Fig. 17c. A comparison of Figs. 17b and c shows that determination of the zero time, within reason, which corresponds to the inflection point, does not have an appreciable effect on the calculated source heat rate.

Two typical temperature-time curves for the black-body cavity with external flow are illustrated in Figs. 18a and b. The exponential equation used for the calculations is presented with the heat sensor curve. The re-radiated heat rate from the surface cap to the heat sensor was calculated using the measured temperatures because of the difficulty of fitting an accurate exponential equation to this curve. The respective calculated heat rate-time histories for the temperature curves in Figs. 18a and b are presented in Figs. 19a and b. The results in Figs. 19a and b indicate that, initially, the black-body cavity was subjected to very high heating rates and then approached equilibrium at the radiant source heat rate

received from the graphite liner. Because the calculated source heat rate in Figs. 19a and b are still in a transient state at the end of the measured time period, an equation of the following form was fitted to the calculated source heat rate

$$Q(\theta) = A + B e^{-Z\theta}$$

and θ was taken to infinite. The equilibrium calculated source heat rate for Figs. 19a and b was, respectively, zero and 600×10^{-6} Btu/sec. The magnitude of the error for the calculated equilibrium versus the actual source heat rate for Figs. 19a and b is not too disconcerting when considering the accuracy necessary to obtain the calculated equilibrium source heat rate after experiencing such a high initial value. The high initial heat rate is not attributed to a mass interchange process as illustrated in Fig. 5 because it is felt that if this phenomenon were predominating, the heat sensor would have obtained much higher temperatures, and the calculated equilibrium source heat rate would have had a value much greater than the actual source radiant heat rate. Rather, the high initial heating rates in Figs. 19a and b are attributed to a large pressure surge of helium gas at near furnace temperature into the cavity when the valve in the external flow simulation tube was opened. This is further evidenced by the fact that the initial temperature rise for both instruments is independent of the fact that the cavity aperture diameters were 0.05 and 0.15 in. in diameter. Fortunately, in testing at a given simulated altitude condition, the source radiant heat rate should remain relatively constant. Therefore, if a pressure surge involving hot gases is encountered during the start transient of a rocket test, the black-body cavity calculated source heat rate can be solved at greater times until a constant value is obtained. Furthermore, for purposes of actual flight tests, in general, missile base pressures initially decrease slowly and then tend to remain relatively constant with time.

One method of improving the current black-body design, as evidenced by the experimental data, would be to replace the metal surface cap with a cap made of an insulating material, such as a ceramic and to use a polished metallic insert as the cavity aperture. This change would serve a two-fold purpose in that it would eliminate an extraneous source of heat to the heat sensing unit and also would limit internal convective currents caused by temperature variations within the cavity.

In all, an aperture diameter of 0.15 in. may be used in conjunction with the black-body cavity and is more desirable than the 0.05-in.-aperture because, for the same cavity internal surface area, the resulting temperature-time history for the same source heat rate will be greater with the 0.15-in. aperture. Thus, the empirical equation used to define the temperature history can be more accurately defined, and also the

absolute effect of the instrument read-out error will be lessened. One-dimensional heat conduction equations may be used to determine insulator losses providing sufficient insulation is used based on the environmental temperature histories and the exposure time period. However, if so desired, it should be possible to improve the accuracy of the results by calculating the insulator losses by the method of finite differences and accounting for the emissivity of the sides of the aperture walls.

6.0 CONCLUDING REMARKS

Some of the methods of measuring heat rates in the base areas of rocket-powered missiles and the inherent errors in these methods are summarized as follows:

1. The use of a polished and blackened slug mass calorimeter to determine convective and radiant heat rates can result in considerable error because of surface contamination on the polished surface caused by the rocket exhaust gases.
2. The practice of embedding a thin disc copper calorimeter in a steel missile base can cause considerable error because of the large change in the base temperature-time history as compared to the temperature-time history of the segment it replaces.
3. When analyzing a slug mass calorimeter, the assumption that the incoming heat rate is equal to the change in internal energy may be greatly in error because of the resultant gains and/or losses of heat through the surrounding insulation.
4. The practice of calibrating a device which will measure convective heat rates in a laboratory with a standard black-body radiant energy source and then comparing experimental results with the calibration to determine heat rates requires that the external environment of the calorimeter be artificially controlled or isolated in order to duplicate the conditions during the calibration. Either of these methods will cause a considerable change in the actual base thermal characteristics with a resultant error because of the effects on the base gas film coefficient.

In this report it has been determined that an embedded slug mass calorimeter and a black-body cavity may be used to obtain reasonably accurate heat transfer measurements in the base areas of rocket-powered missiles if an analytic heat balance is written about the heat sensing unit.

When using these devices to measure heating rates, the following practices should be observed:

1. Preliminary analysis to properly size and design the measuring devices. (One of the prime considerations in the design should be to facilitate the mathematical analysis.)
2. Measurement of each instrument to determine the heat transfer areas required for the mathematical computations.
3. Individual weight determination of the calorimeter and cavity heat sensing unit.
4. Extreme care in instrumentation and data reduction procedures.

REFERENCES

1. Sitnik, G. F. "General Principles for the Realization of a Model of a Black-Body at a High Temperature." Translated from: Astronomecheskii Zhurnal, Vol. 37, No. 1, pp 75-85, January - February, 1960.
2. Simmons, F. S., DeBell, A. G., and Anderson, Q. S. "A 2000°C Slit-Aperture Black-Body Source." Review of Scientific Instruments, 32, 1265 (1961).
3. Glawe, G. E., Simmons, F. S., and Stickney, T. M. "Radiation and Recovery Corrections and Time Constants of Several Chromel-Alumel Thermocouple Probes in High-Temperature, High-Velocity Gas Streams." NACA TN 3766, October 1956.
4. Freeze, P. D. "Bibliography on the Measurement of Gas Temperatures." Circular 513, National Bureau of Standards, August 20, 1951.
5. Bendersky, D. "A Special Thermocouple for Measuring Transient Temperatures." Mechanical Engineering, February, 1953.
6. Westkaemper, J. C. "An Analysis of Slug-Type Calorimeters for Measuring Heat Transfer from Exhaust Gases." AEDC-TN-60-202, November 1960.
7. Westkaemper, J. C. "On the Error in Slug-Type Calorimeters Caused by Surface-Temperature Mismatch." Journal of the Aerospace Sciences, November 1961.
8. Cresci, R. J. and Libby, P. A. "Some Heat Conduction Solutions Involved in Transient Heat Transfer Measurements." WADC-TN-57-236, September 1957.

9. Dusinberre, G. M. Numerical Analysis of Heat Flow. McGraw-Hill, New York, 1949.
10. Freed, N. H. and Rallis, C. J. "Truncation Error Estimates for Numerical and Analog Solutions of the Heat-Conduction Equation." Journal of Heat Transfer, p 382, August 1961.
11. Carslaw, H. S. and Jaeger, J. C. Conduction of Heat in Solids. Oxford at the Clarendon Press, London, 1950.
12. Walker, R. E. and Grenleski, S. E. "Instrument for Measuring Total Incident Radiant Heat Transfer to a Jet Engine Surface." ARS Journal, January 1961.
13. Gouffe, A. "Corrections d'Ouverture des Corps-Noirs Artificiels Compte Tenu des Diffusions Multiple Internes." Revue D'Optique, January - March, 1945.
14. Buschman, A. J. and Pittman, C. M. "Configuration Factors for Exchange of Radiant Energy between Axisymmetrical Sections of Cylinders, Cones, and Hemispheres and Their Bases." NASA TN D-944, October 1961.
15. Faddeyeva, V. N. and Terentev, N. M. Tables of the Probability Integral for Complex Argument. Pergamon Press, London, 1961.
16. Jakob, M. Heat Transfer. Volume II, John Wiley and Sons, Incorporated, New York, 1957.
17. Lalos, G. T., Corruccini, R. J., and Broida, H. P. "Design and Construction of a Black-Body and Its Use in the Calibration of a Grating Spectroradiometer." The Review of Scientific Instruments, Volume 29, No. 6, June 1958.
18. McAdams, W. H. Heat Transmissions. McGraw-Hill Book Company, Incorporated, New York, 1954.
19. "Thermophysical Properties of Thermal Insulating Materials." Technical Documentary Report No. ASD-TDR-62-215, July 1962.

TABLE 1

THERMAL PROPERTIES USED FOR THE EXPERIMENTAL PROGRAM

Material	Density, lb_m/ft^3	Conductivity, $\text{Btu}/\text{ft}^2\text{-hr-deg}/\text{ft}$	Specific Heat, $\text{Btu}/\text{lb}_m\text{-deg}$
Polytrifluorochloroethylene Plastic	135	0.035 - 0.07 at (550 - 780°R)	0.22 - 0.27 at(550 - 780°R)
Iron	492	36	0.106
Constantan	555	13	0.102
Stainless Steel Type 347			0.13
Copper			0.094

TABLE 2

PHYSICAL CONSTANTS USED FOR THE BLACK-BODY CAVITY

Aperature, in.	Area (A_1), ft^2	Area (A_4), ft^2	Surface Area (A_D), ft^2	Diameter (D_1), ft	Heat Sensor, Mass, grams
0.05	1.363×10^{-5}	3.271×10^{-4}	1.6×10^{-3}	2.083×10^{-2}	0.597
0.15	1.2266×10^{-4}	2.1805×10^{-4}	1.6×10^{-3}	2.083×10^{-2}	0.582

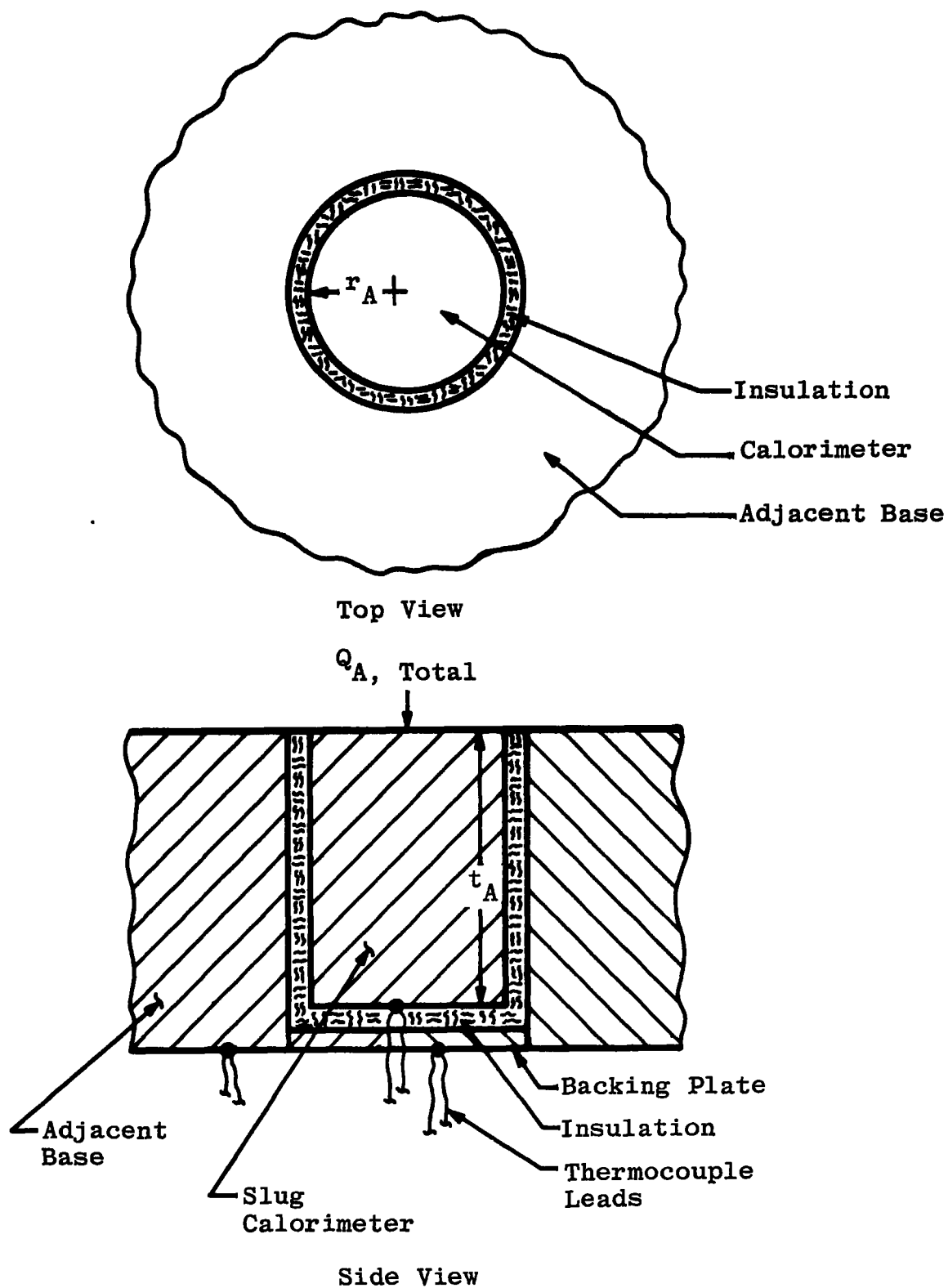


Fig. 1 Slug Mass Calorimeter

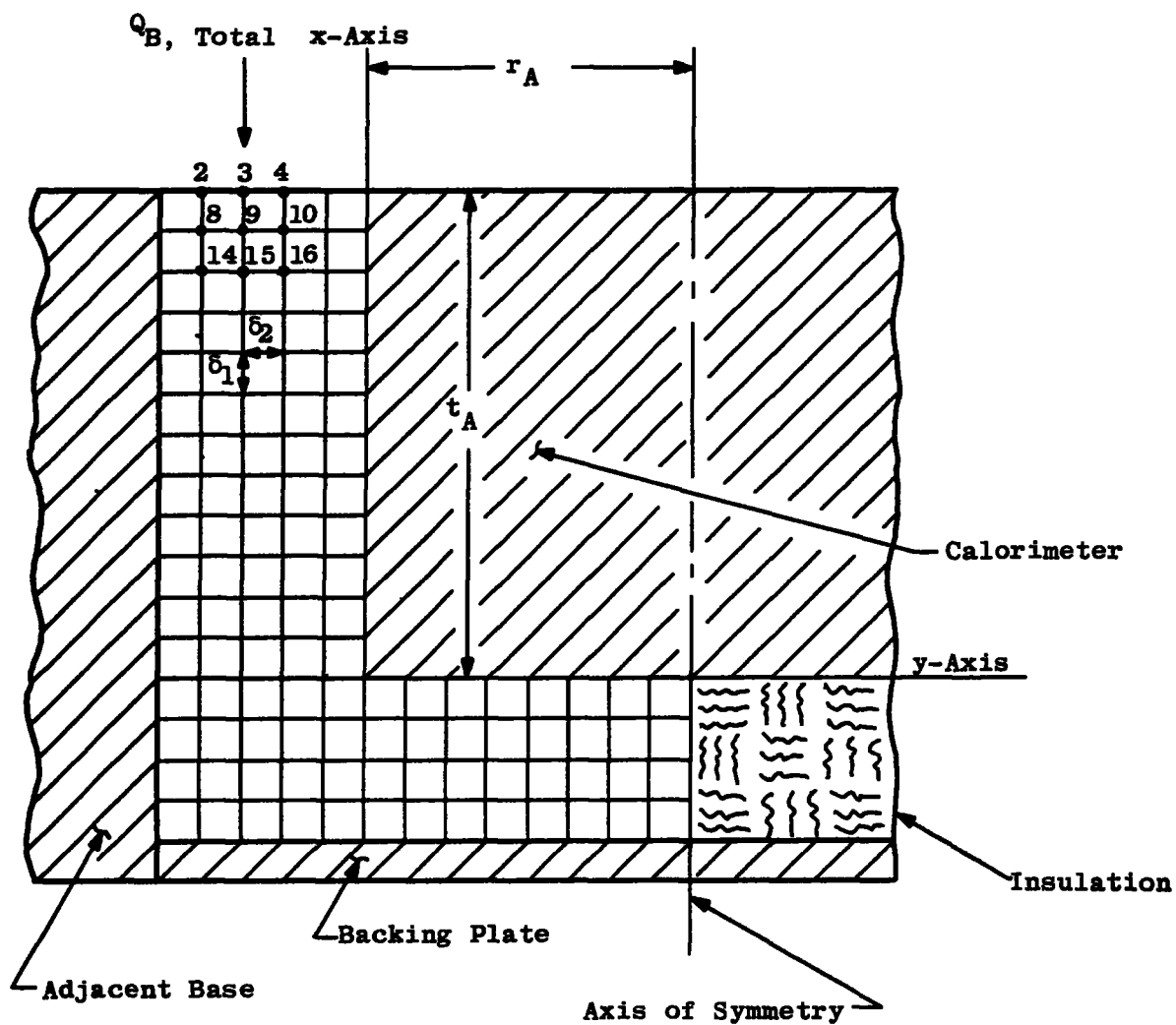
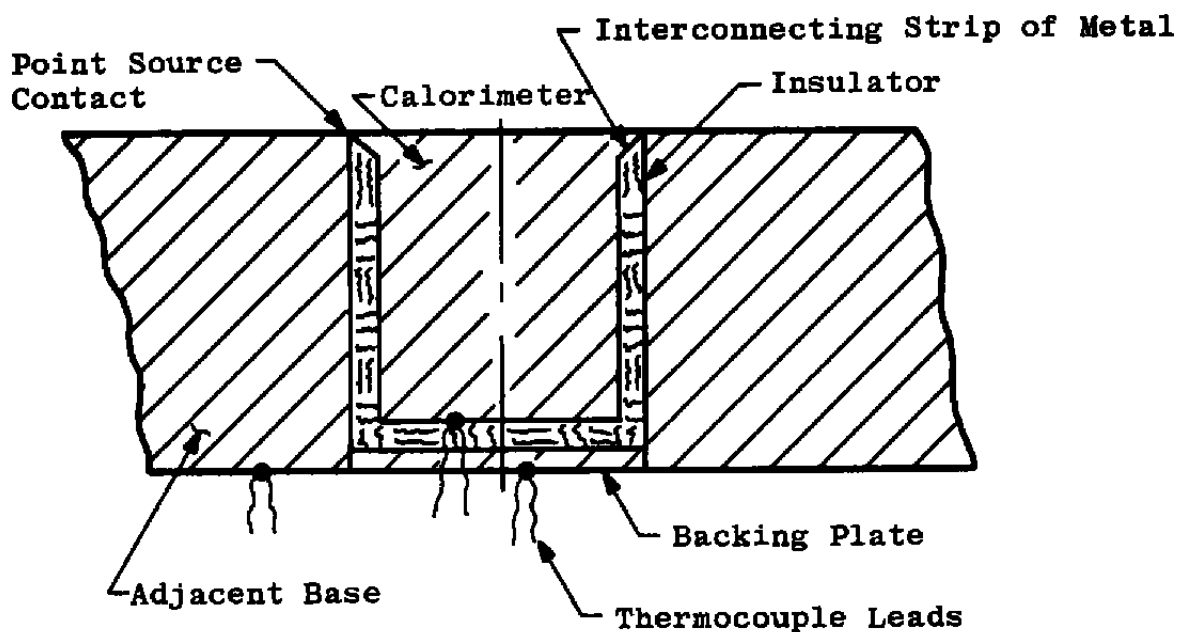
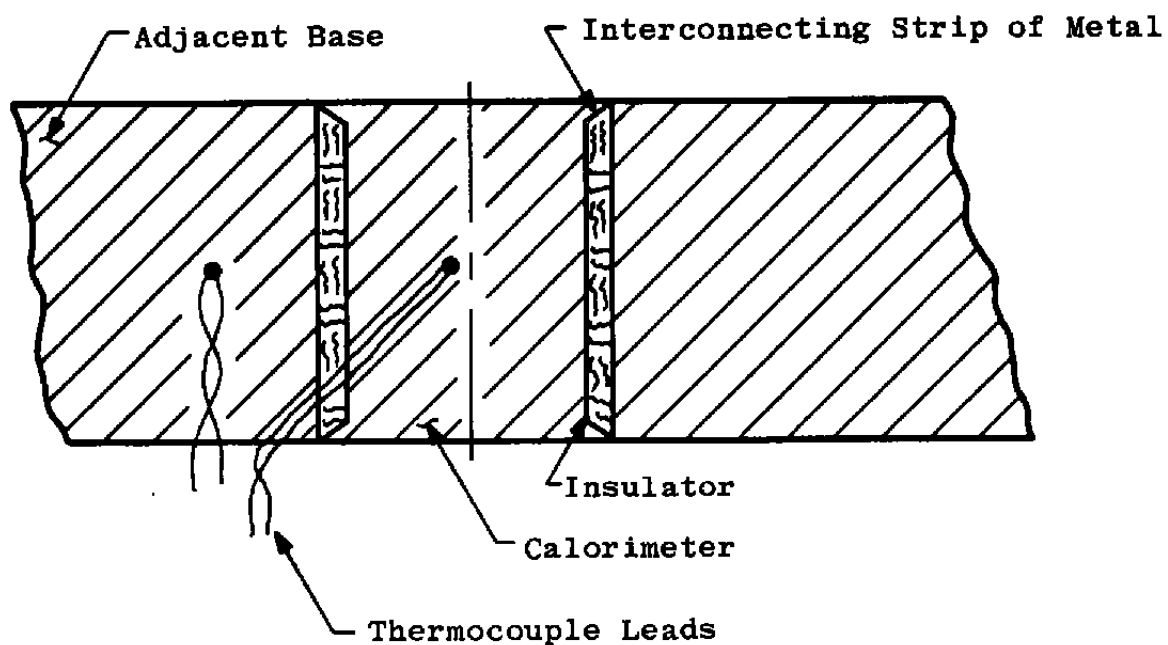


Fig. 2 Two-Dimensional Grid-Network for Calorimeter Insulation



a. Surface Heat Transfer Measurements



b. Surface and Back Heat Transfer Measurements

Fig. 3 Slug Mass Calorimeters

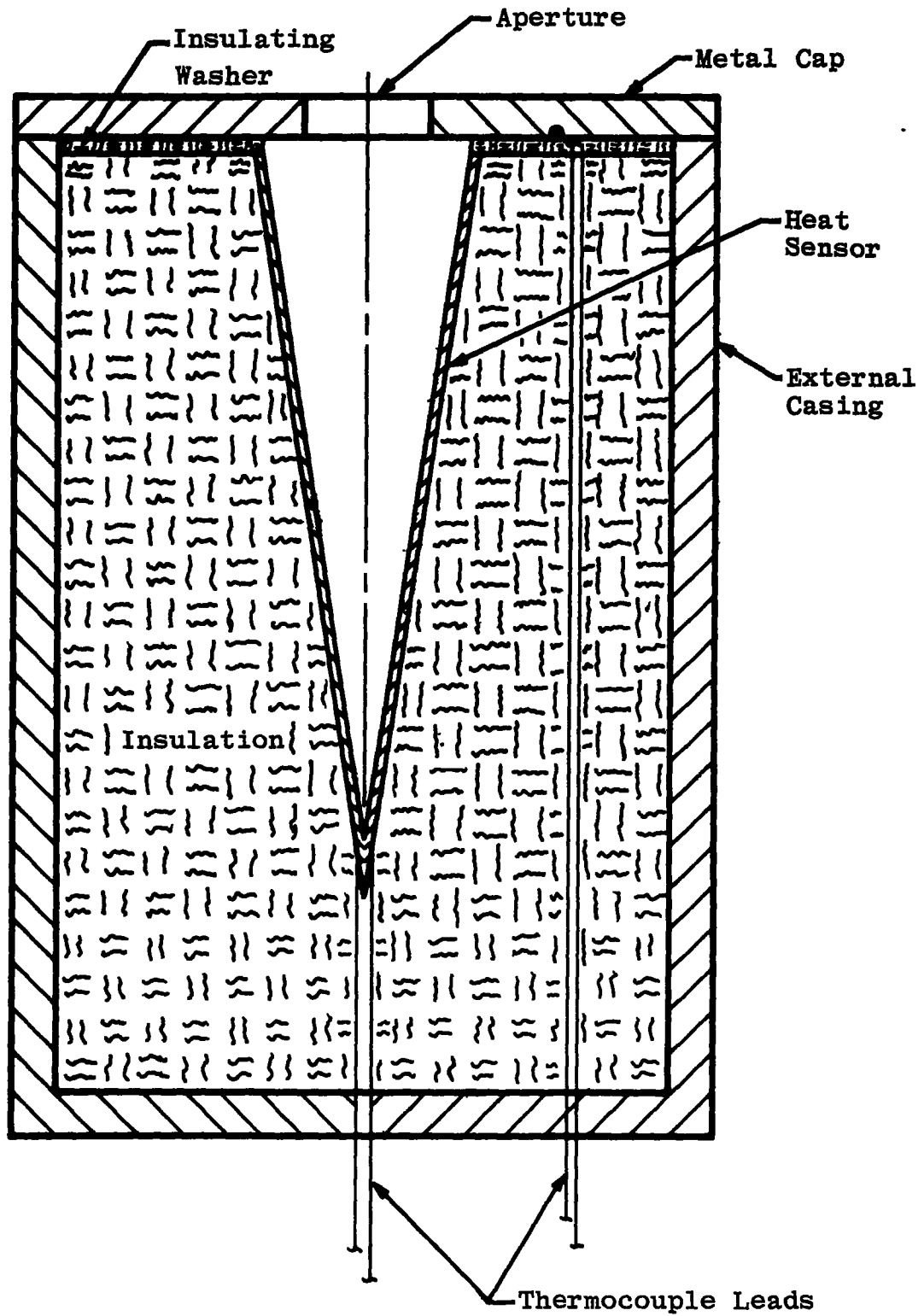


Fig. 4 Black-Body Cavity

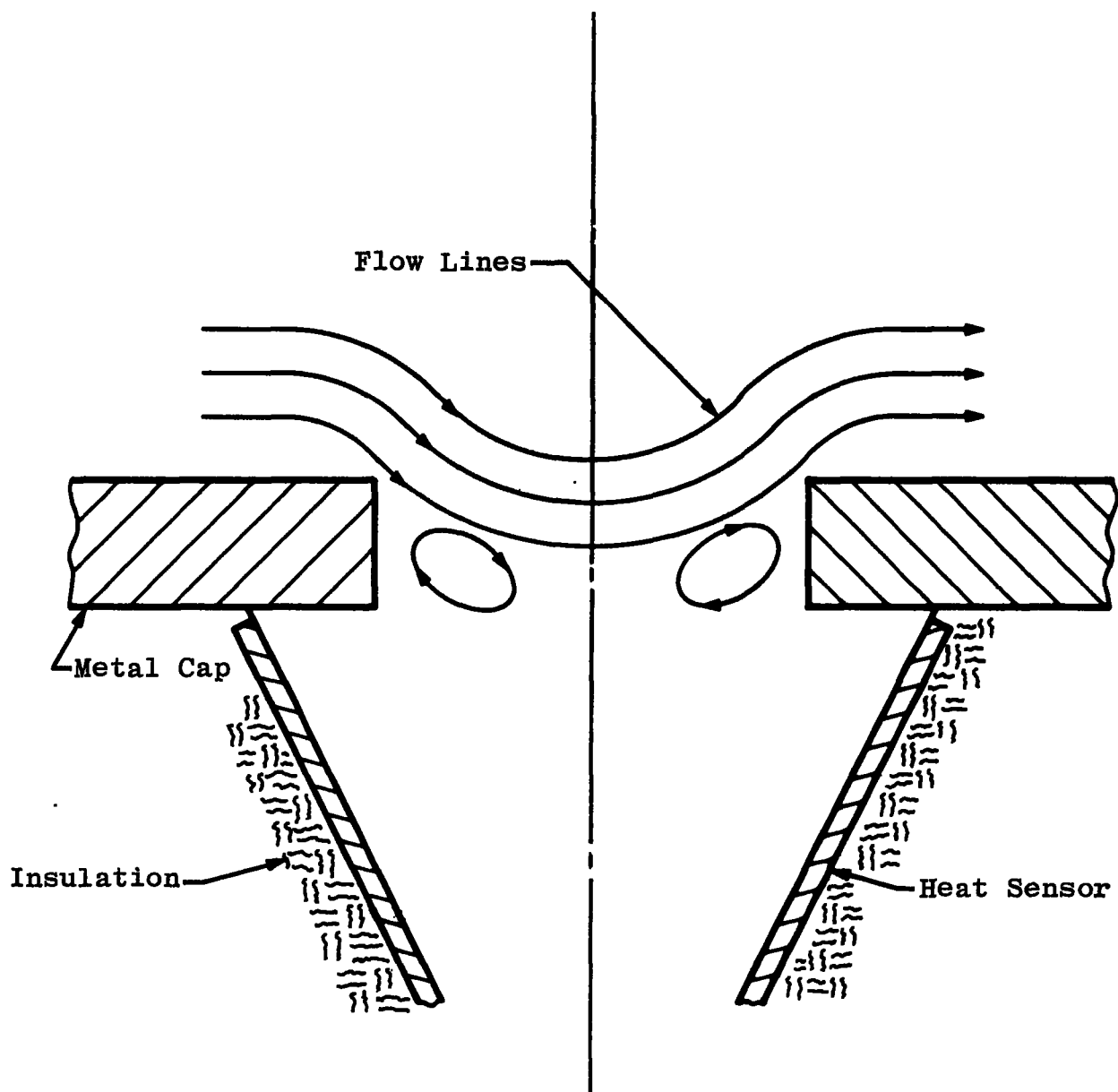


Fig. 5 External Flow Field over Cavity Aperture

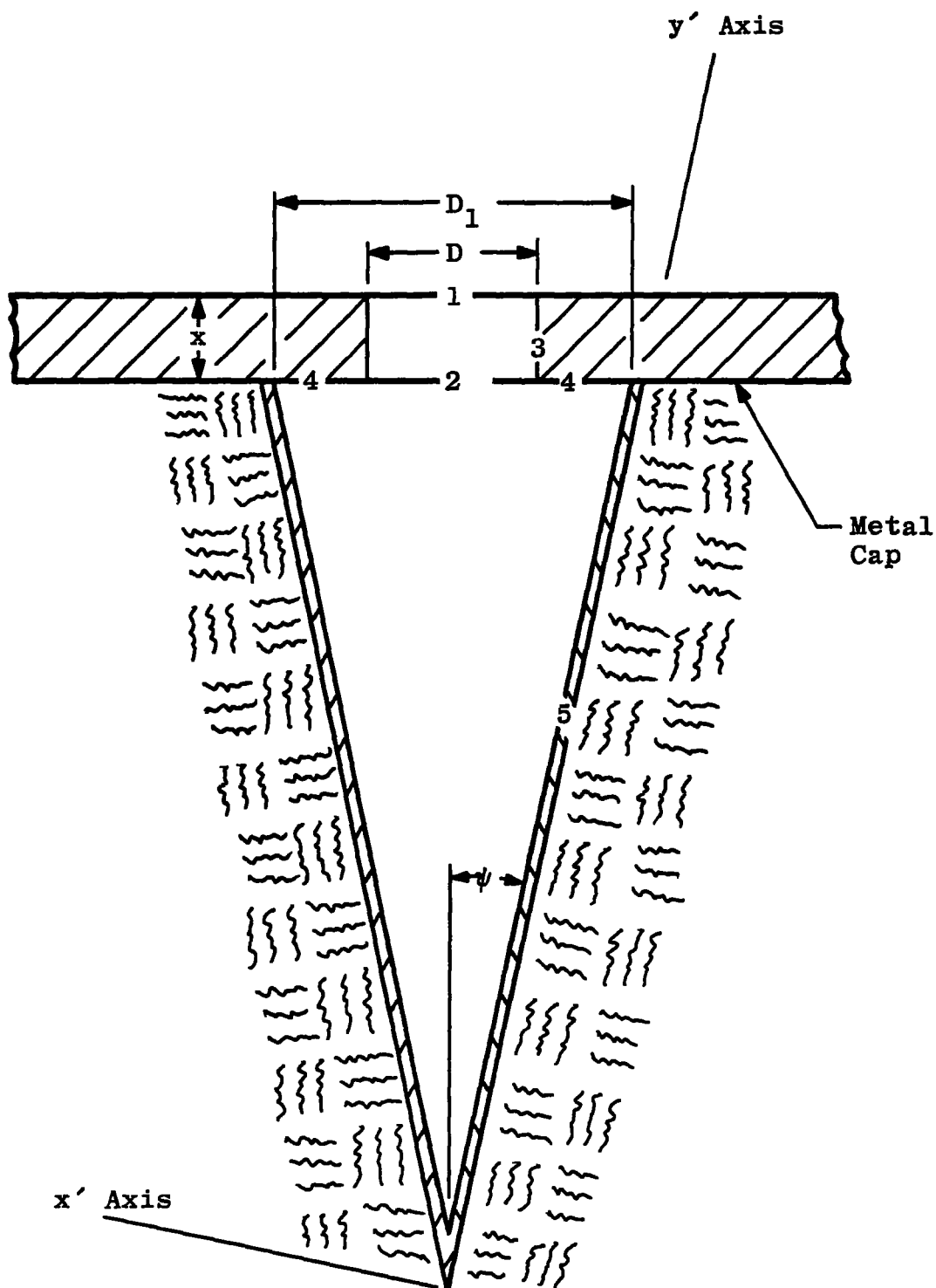


Fig. 6 Identification of Black-Body Cavity Parts

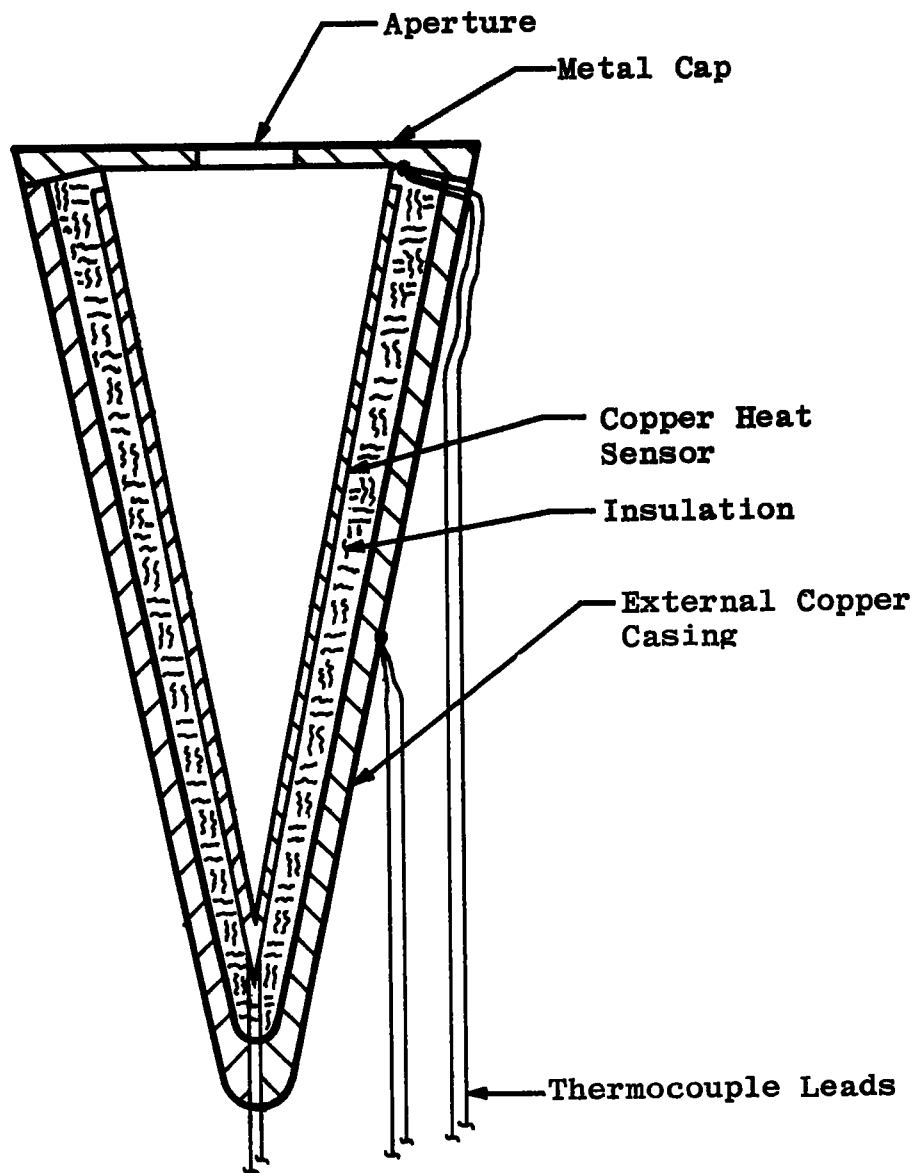


Fig. 7 Black-Body Cavity (High Heat Rates)

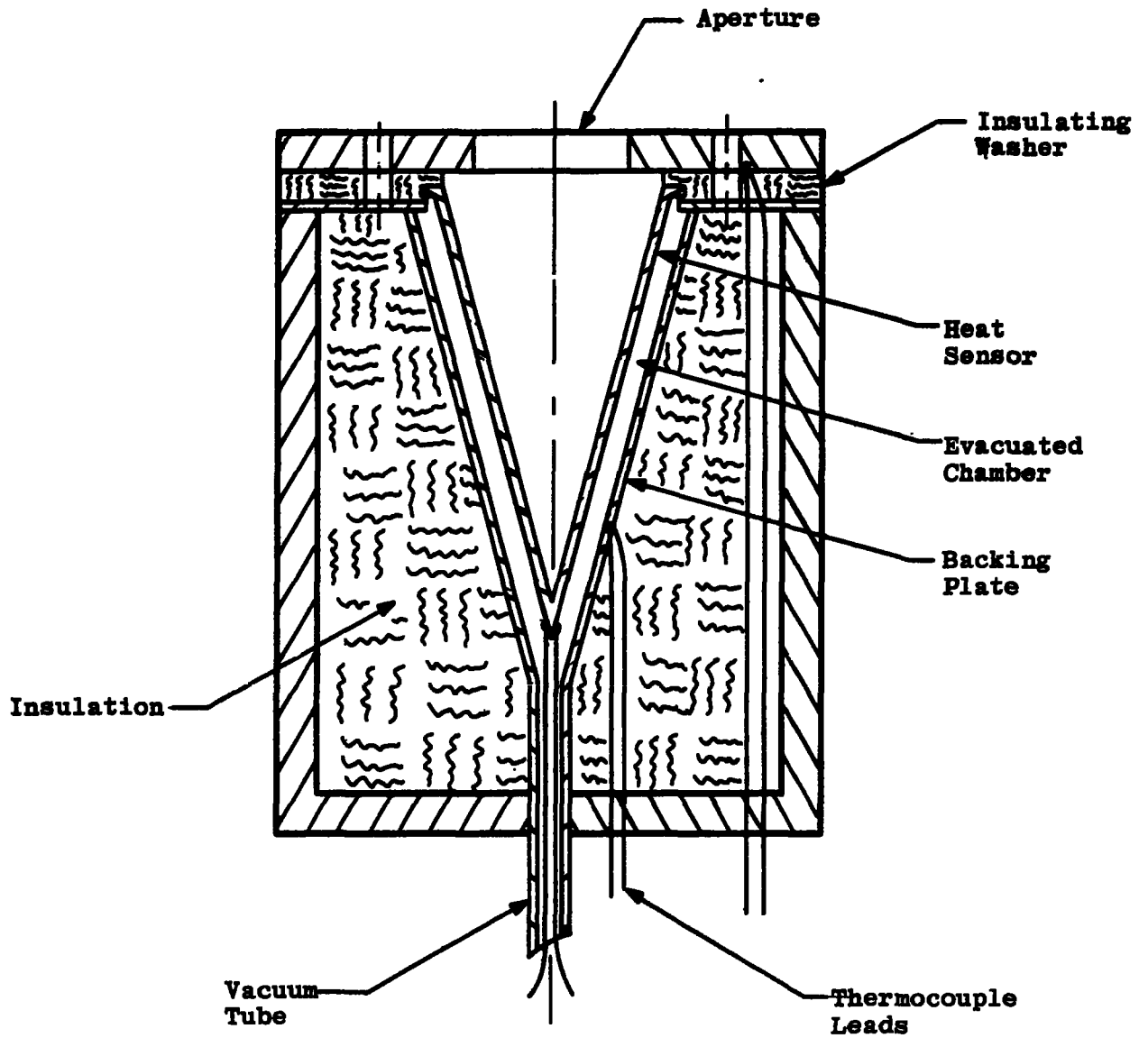


Fig. 8 Black-Body Cavity (Low Heat Rates)

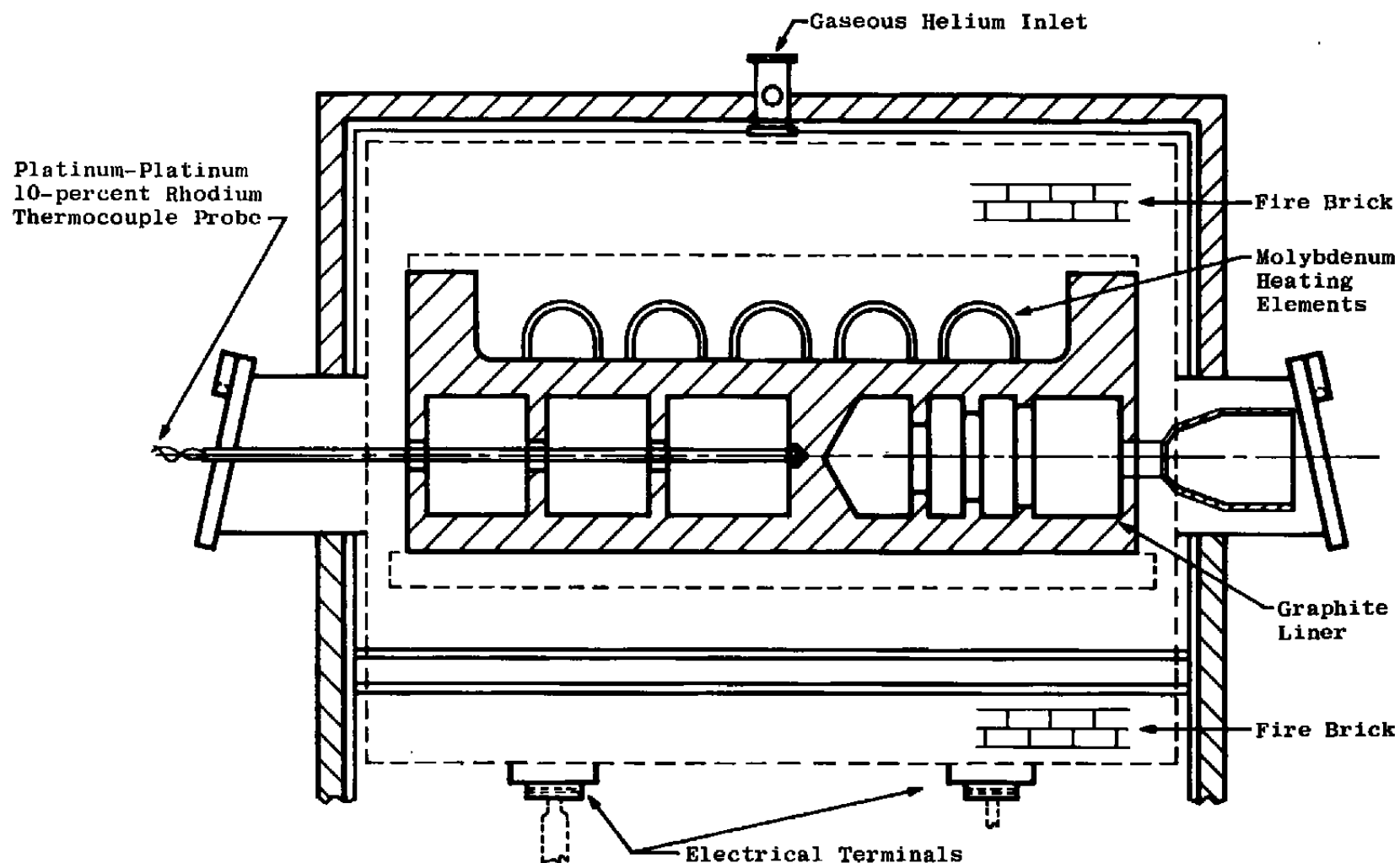


Fig. 9 Experimental Black-Body Radiation Source

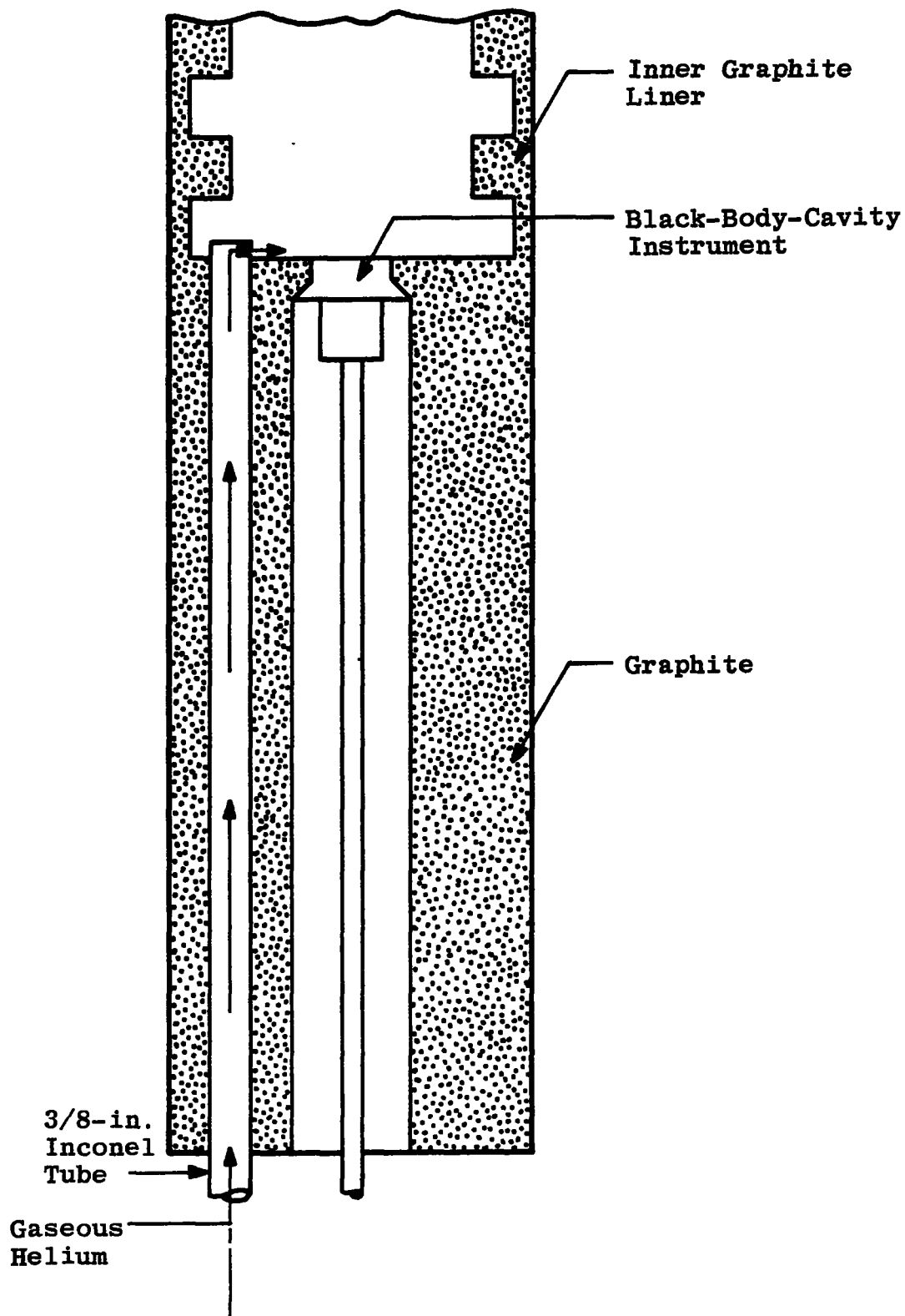


Fig. 10 External Forced Convection Simulation Tube

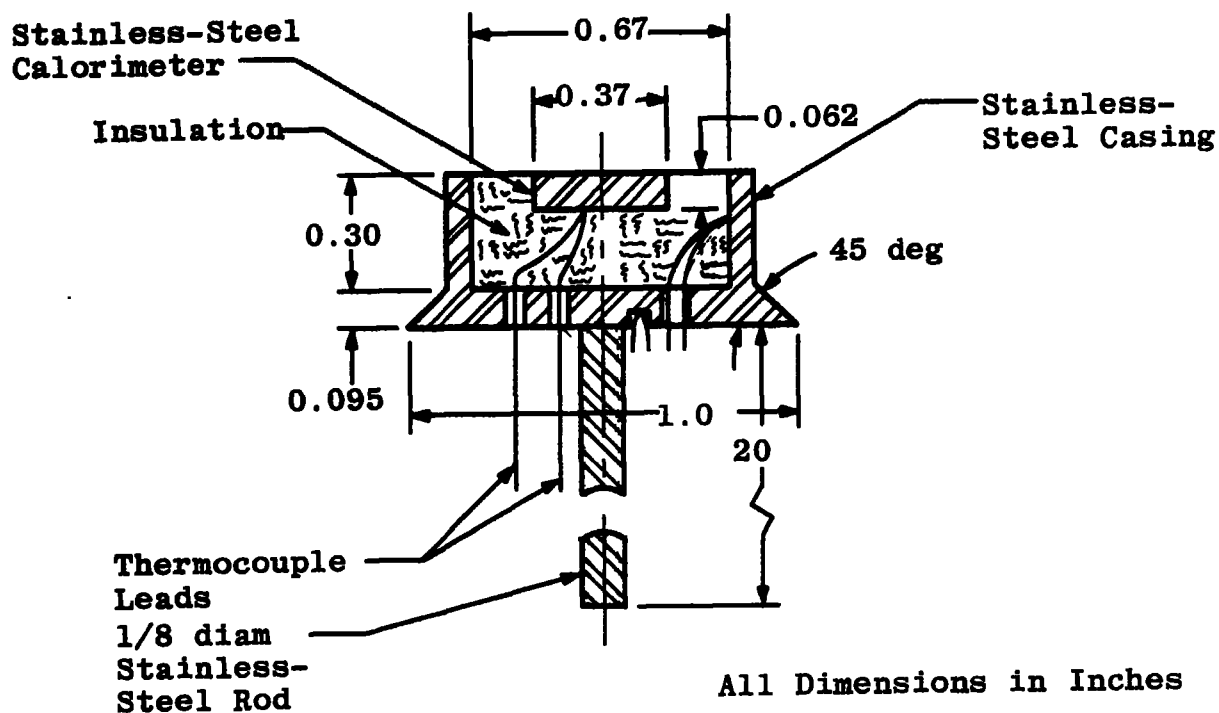


Fig. 11 Experimental Slug Mass Calorimeter

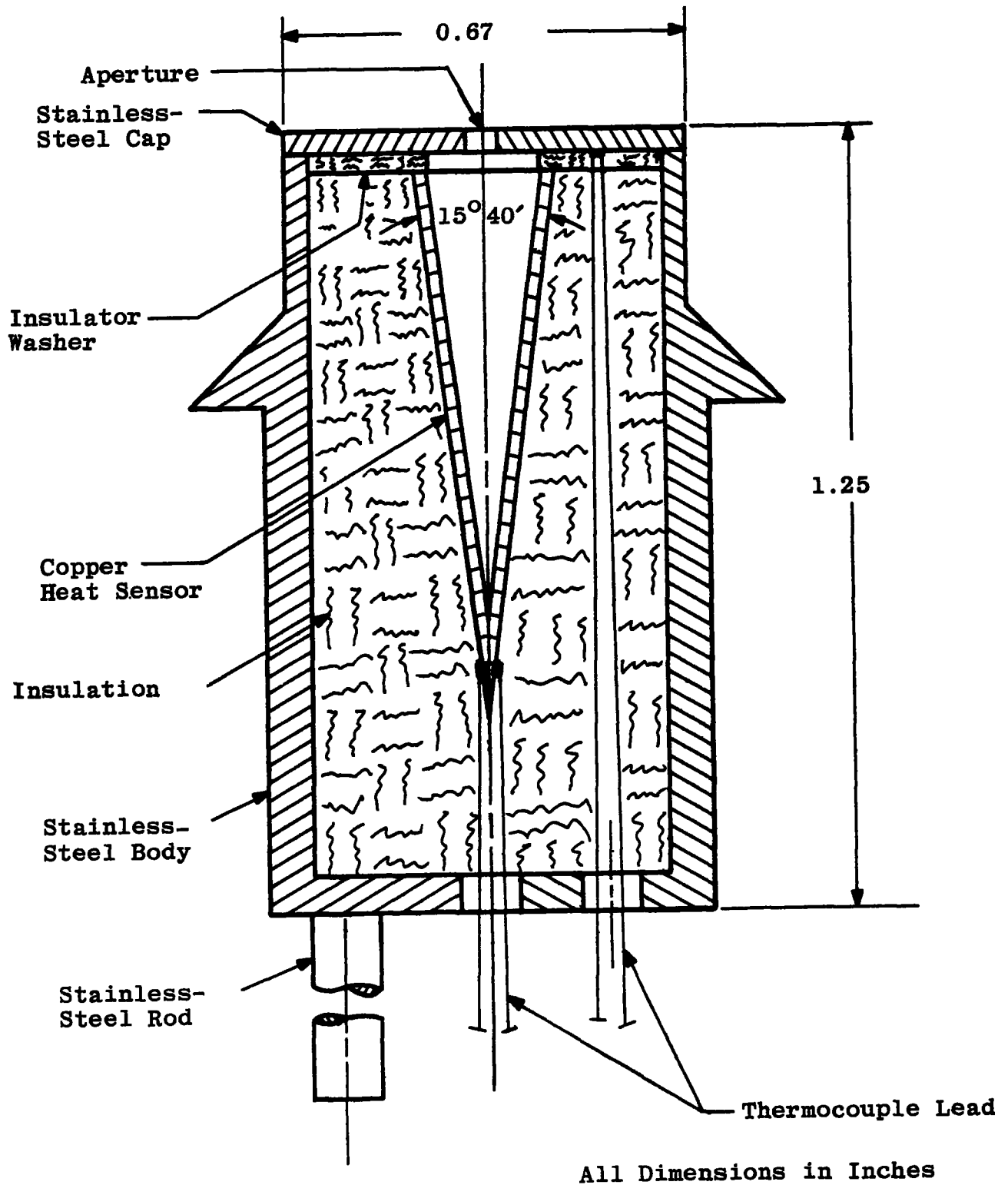


Fig. 12 Experimental Black-Body Cavity

Calorimeter Mass = 0.811 grams

Furnace Temperature = 1960°R

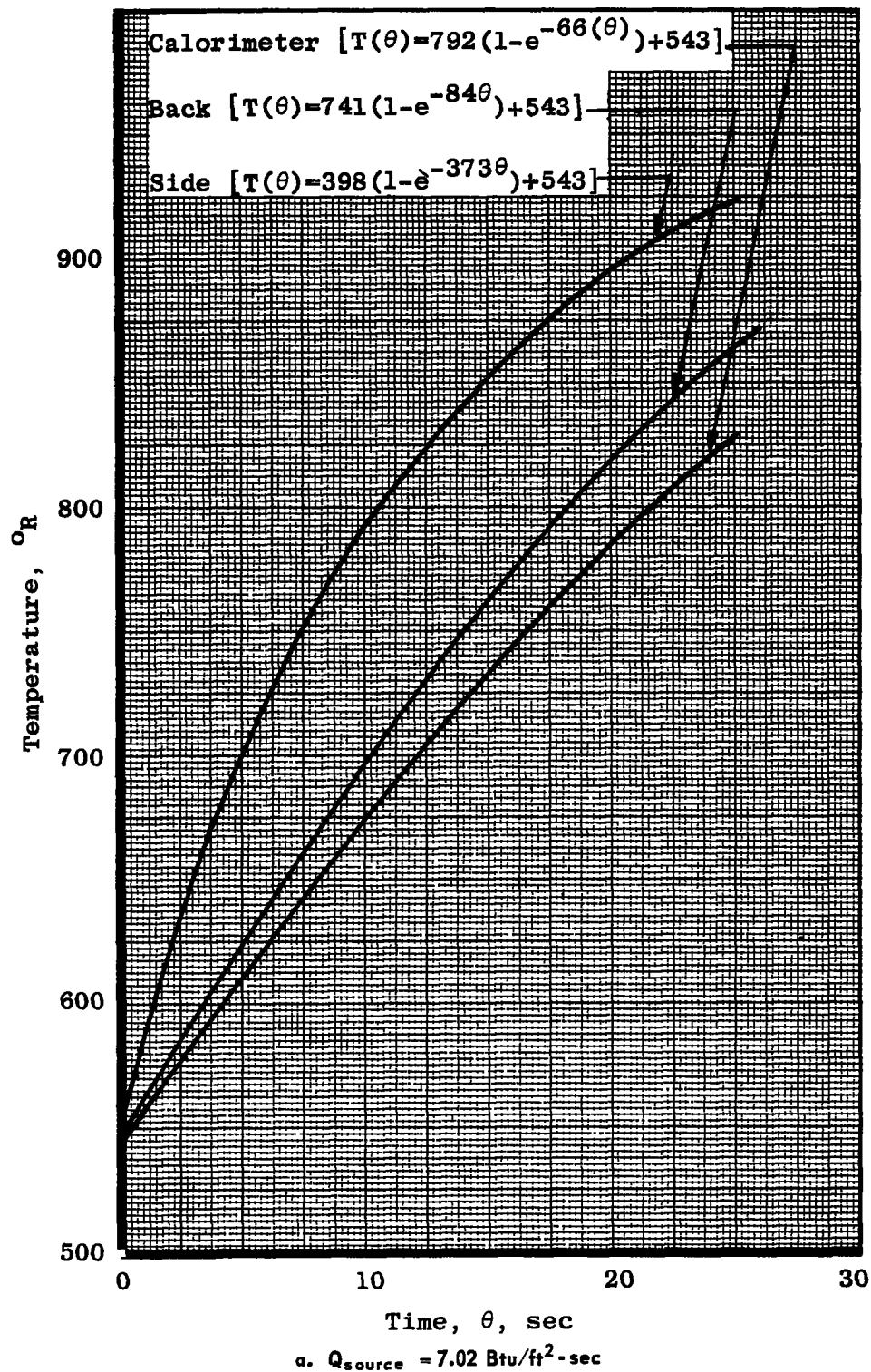
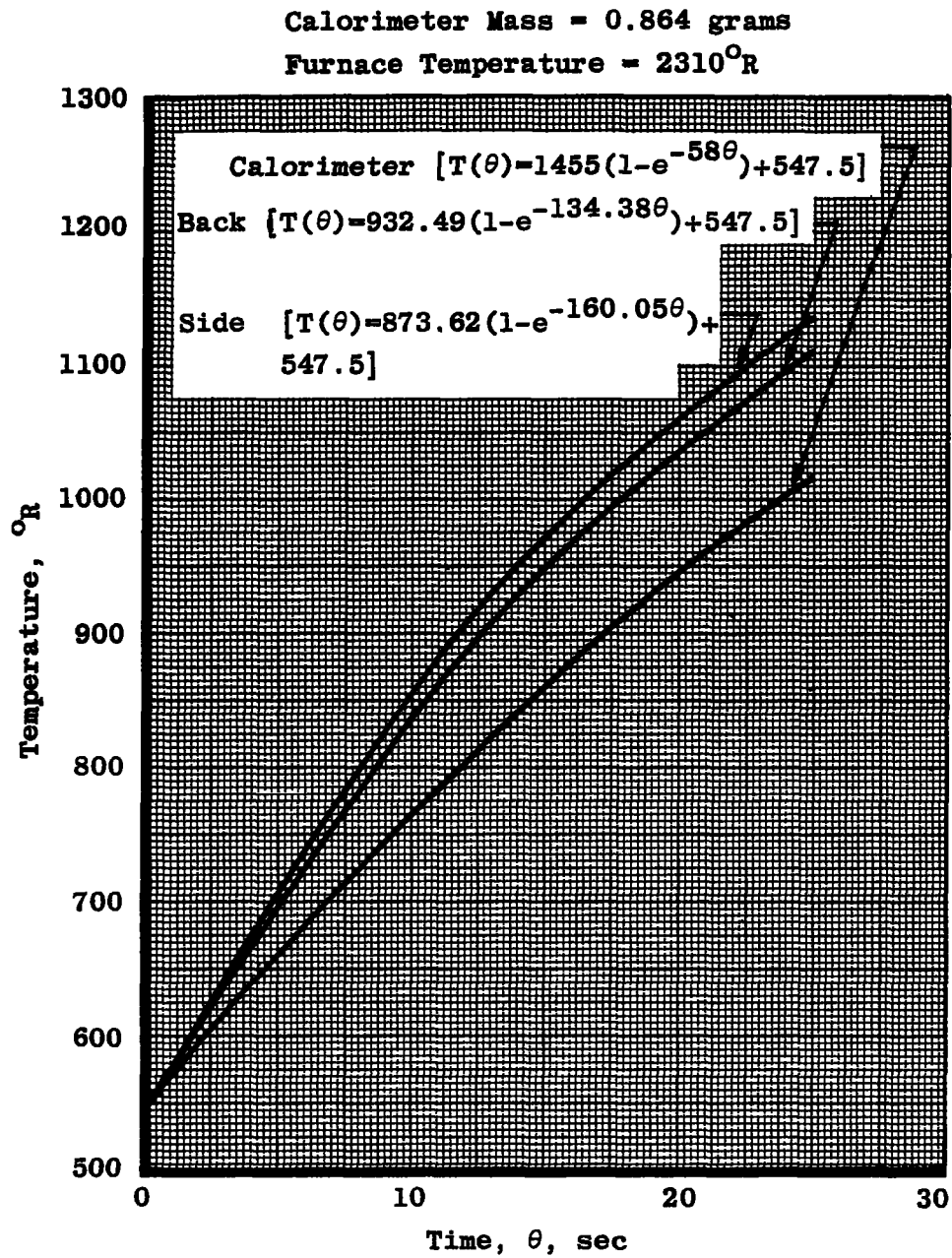


Fig. 13 Calorimeter Temperature-Time Histories



b. $Q_{\text{source}} = 13.55 \text{ Btu/ft}^2\text{-sec}$

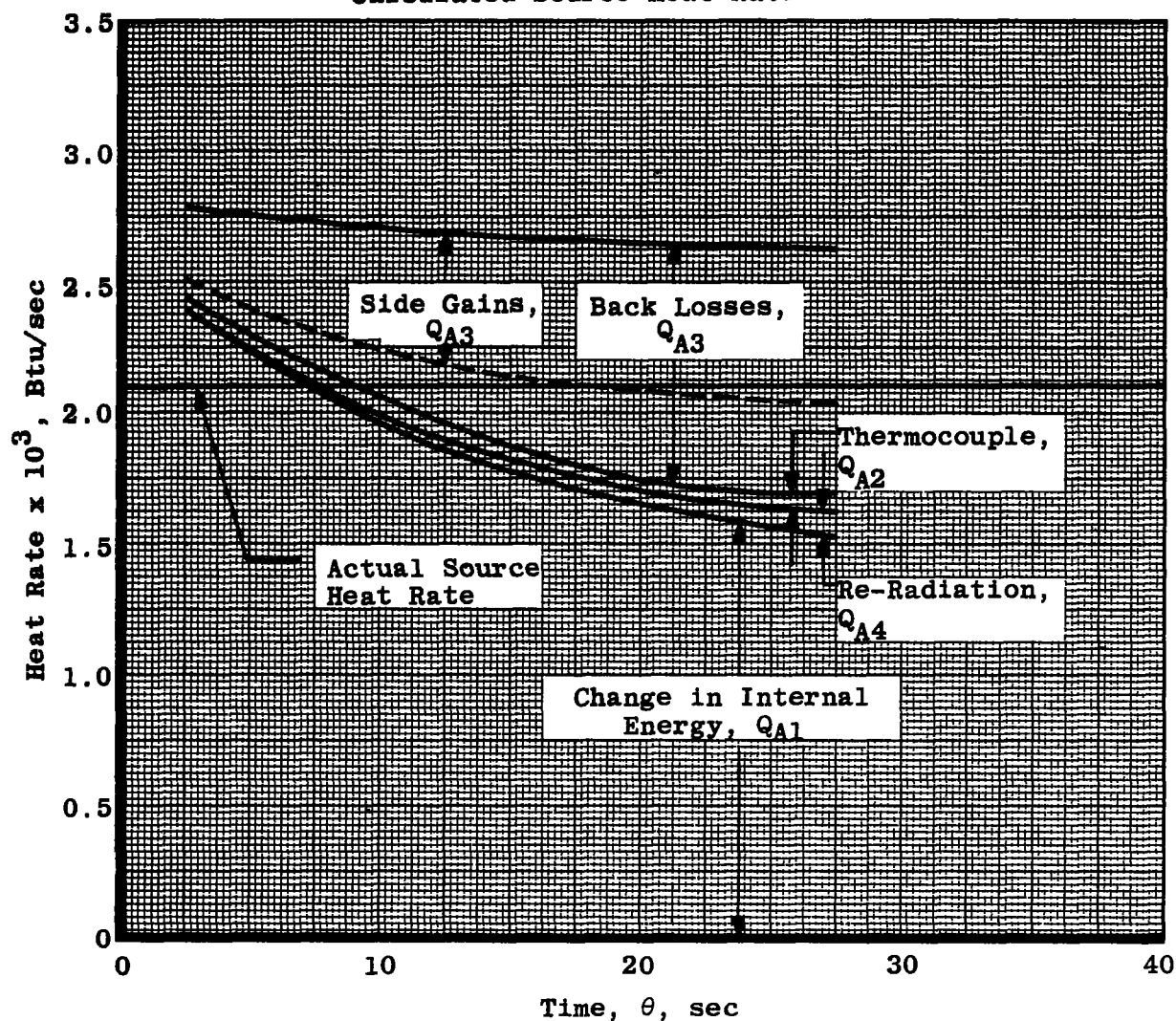
Fig. 13 Concluded

Surface Area of Calorimeter = $7.466 \times 10^{-4} \text{ ft}^2$

$K_B = 0.05 \text{ Btu/ft}^2\text{-hr-deg/ft}$

$C_{pB} = 0.25 \text{ Btu/lb}_m\text{-deg}$

----- Calculated Source Heat Rate



a. $Q_{\text{source}} = 7.02 \text{ Btu/ft}^2\text{-sec}$

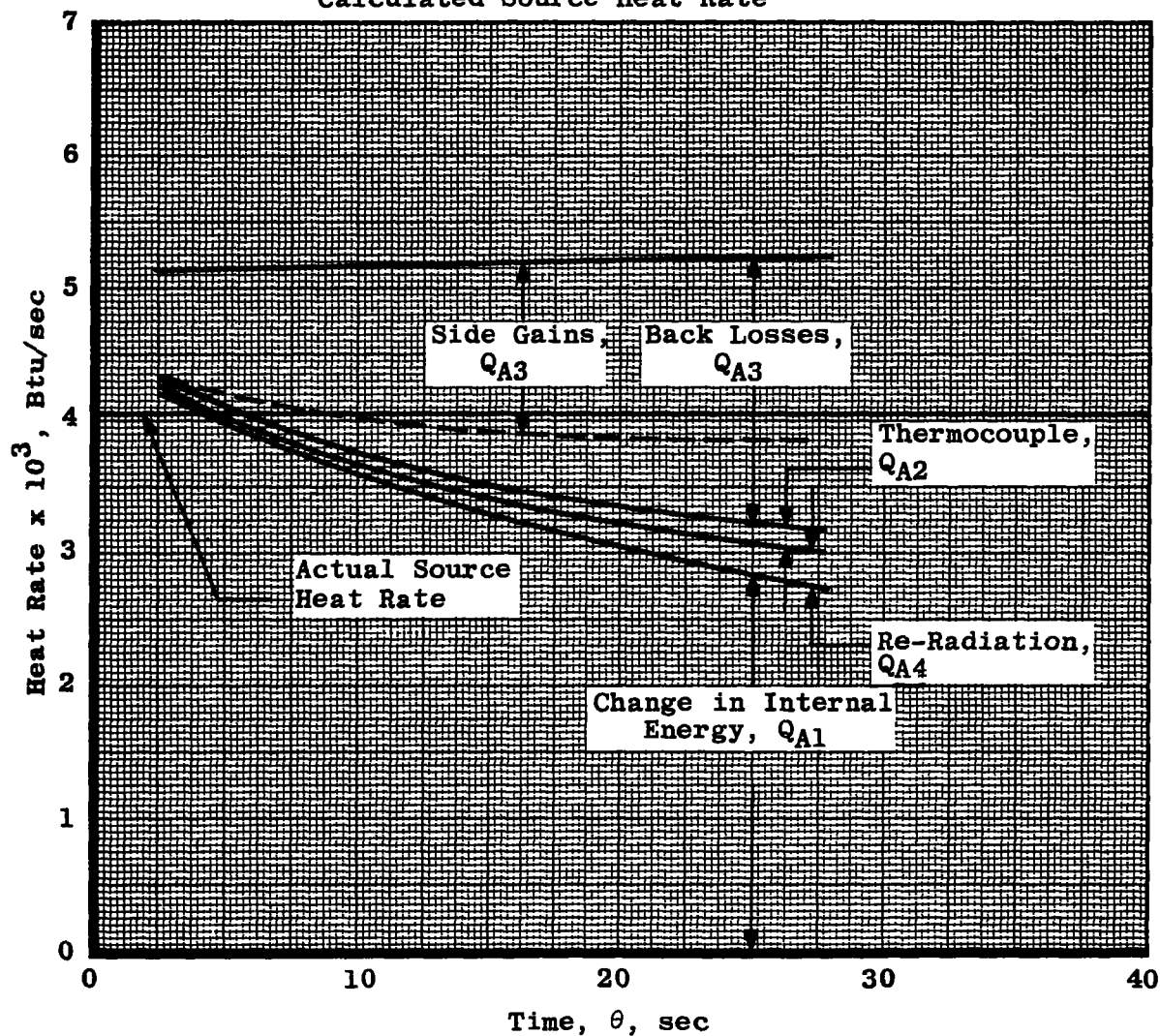
Fig. 14 Calorimeter Heat Rate-Time Histories

Surface Area of Calorimeter = $7.466 \times 10^{-4} \text{ ft}^2$

$K_B = 0.07 \text{ Btu/ft}^2\text{-hr-deg/ft}$

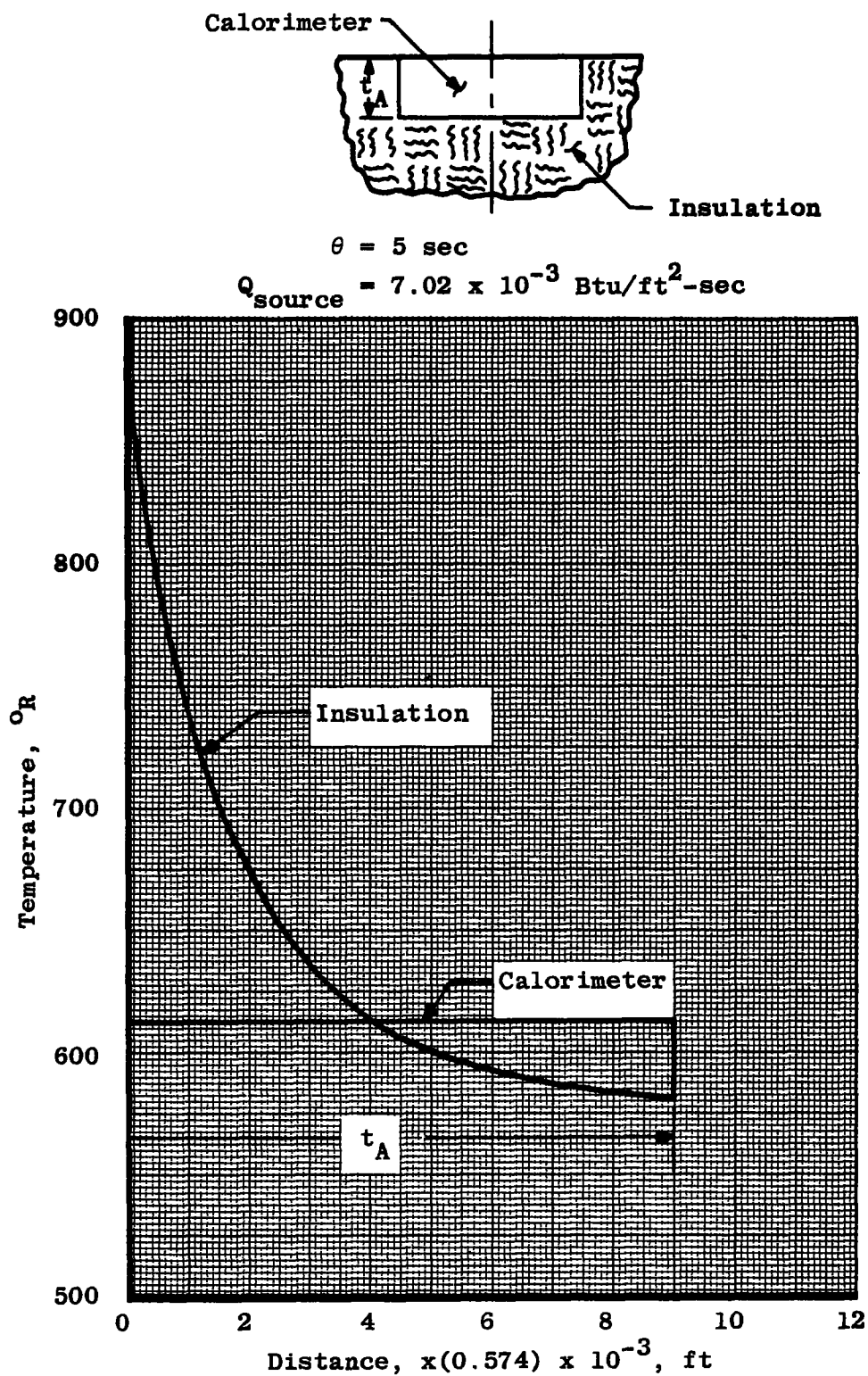
$C_{pB} = 0.27 \text{ Btu/lb}_m\text{-deg}$

----- Calculated Source Heat Rate



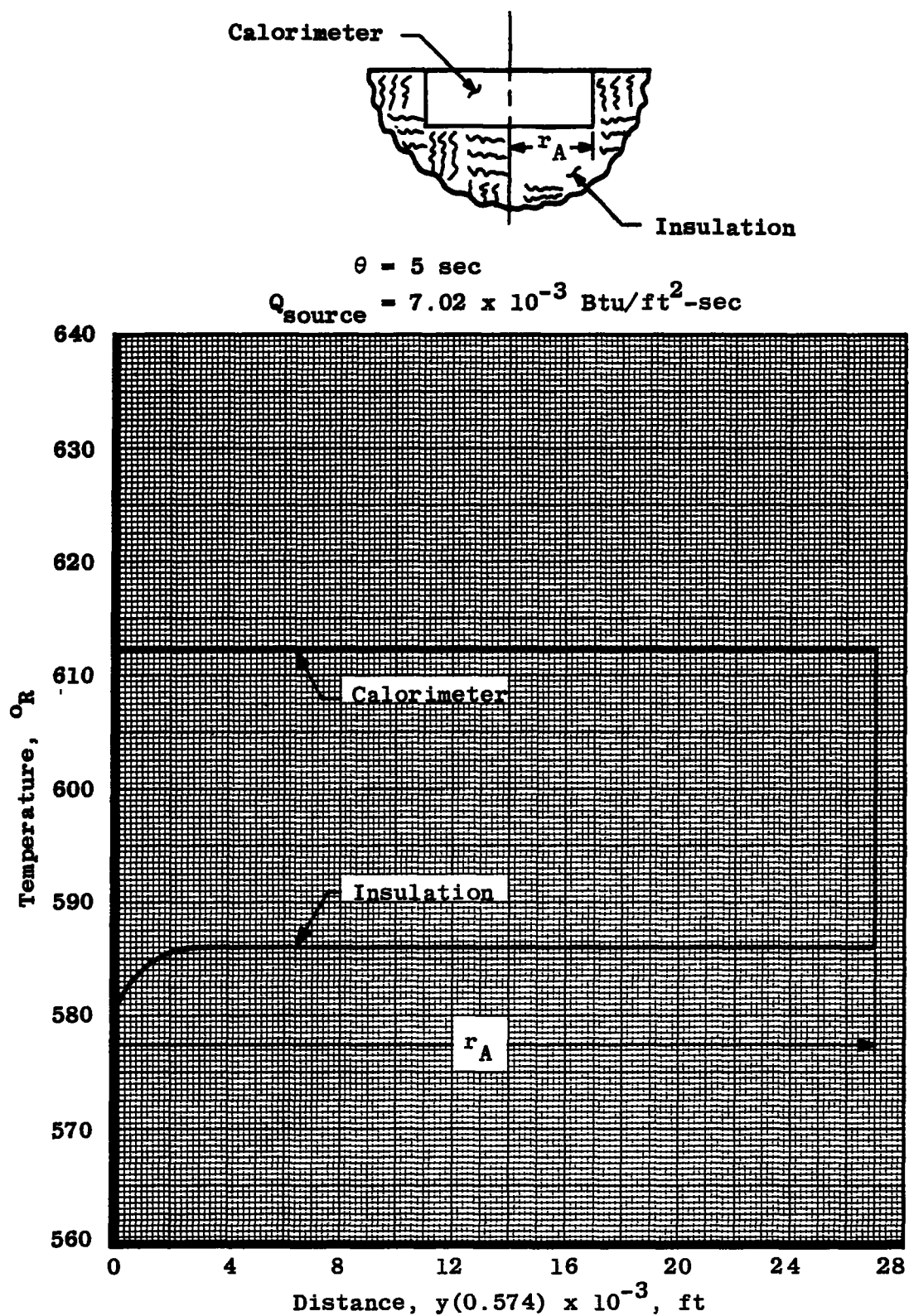
b. $Q_{\text{source}} = 13.55 \text{ Btu/ft}^2\text{-sec}$

Fig. 14 Concluded



a. Side Temperature Distribution

Fig. 15 Typical Temperature Distributions in the Insulator Adjacent to the Calorimeter



b. Back Temperature Distribution

Fig. 15 Concluded

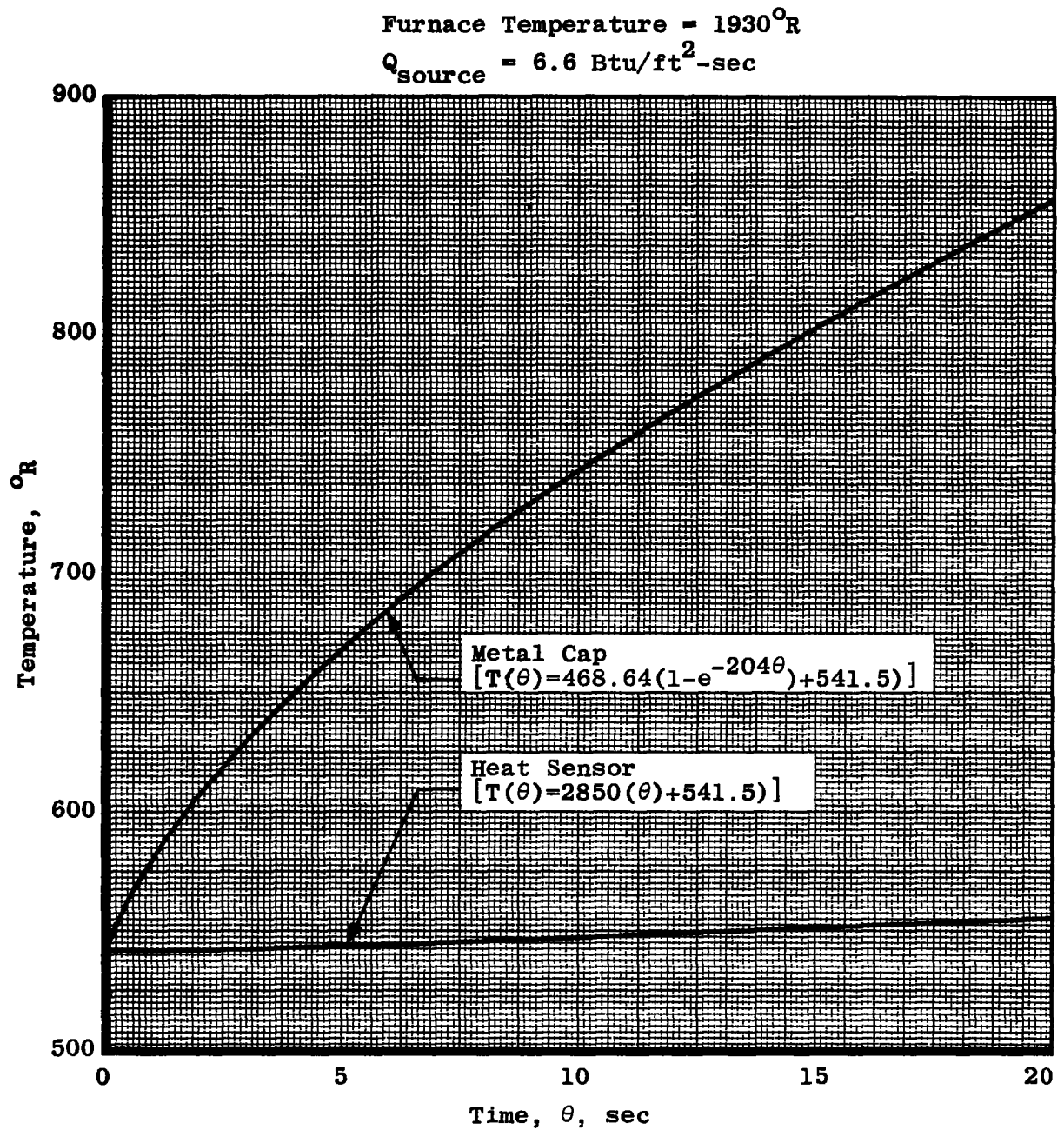
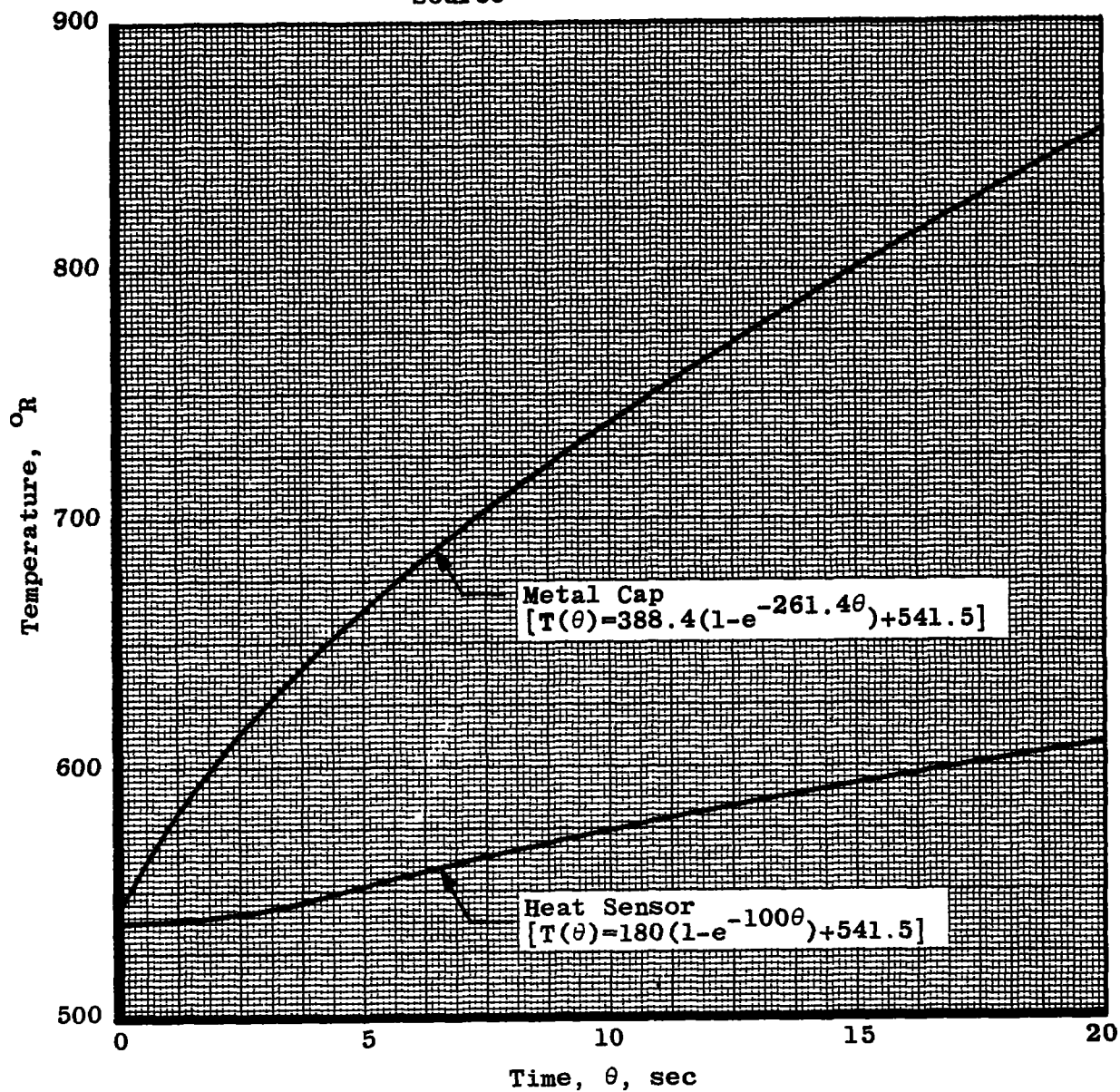


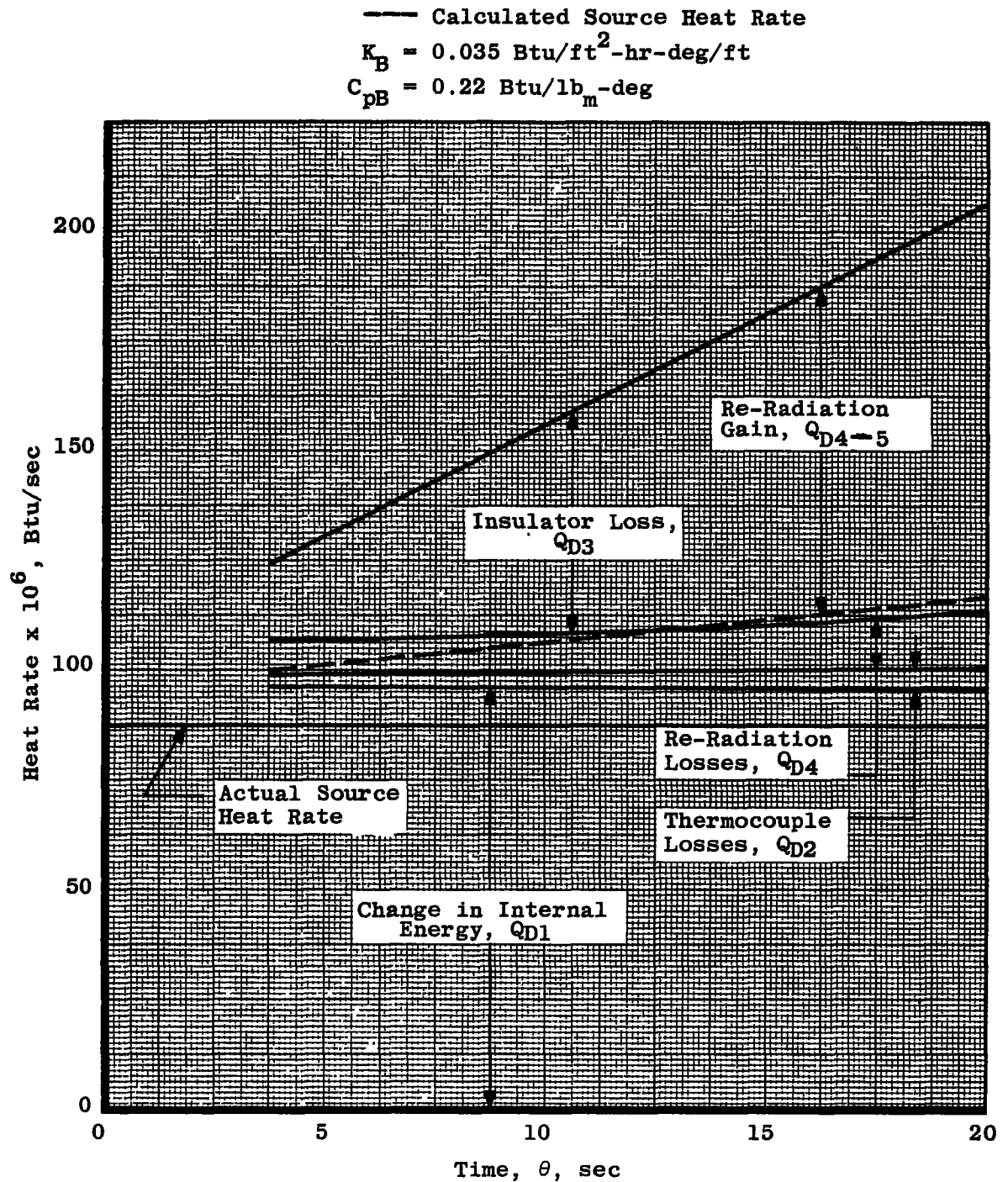
Fig. 16 Black-Body Cavity Temperature-Time Histories

Furnace Temperature = 1914°R
 $Q_{\text{source}} = 6.39 \text{ Btu/ft}^2\text{-sec}$



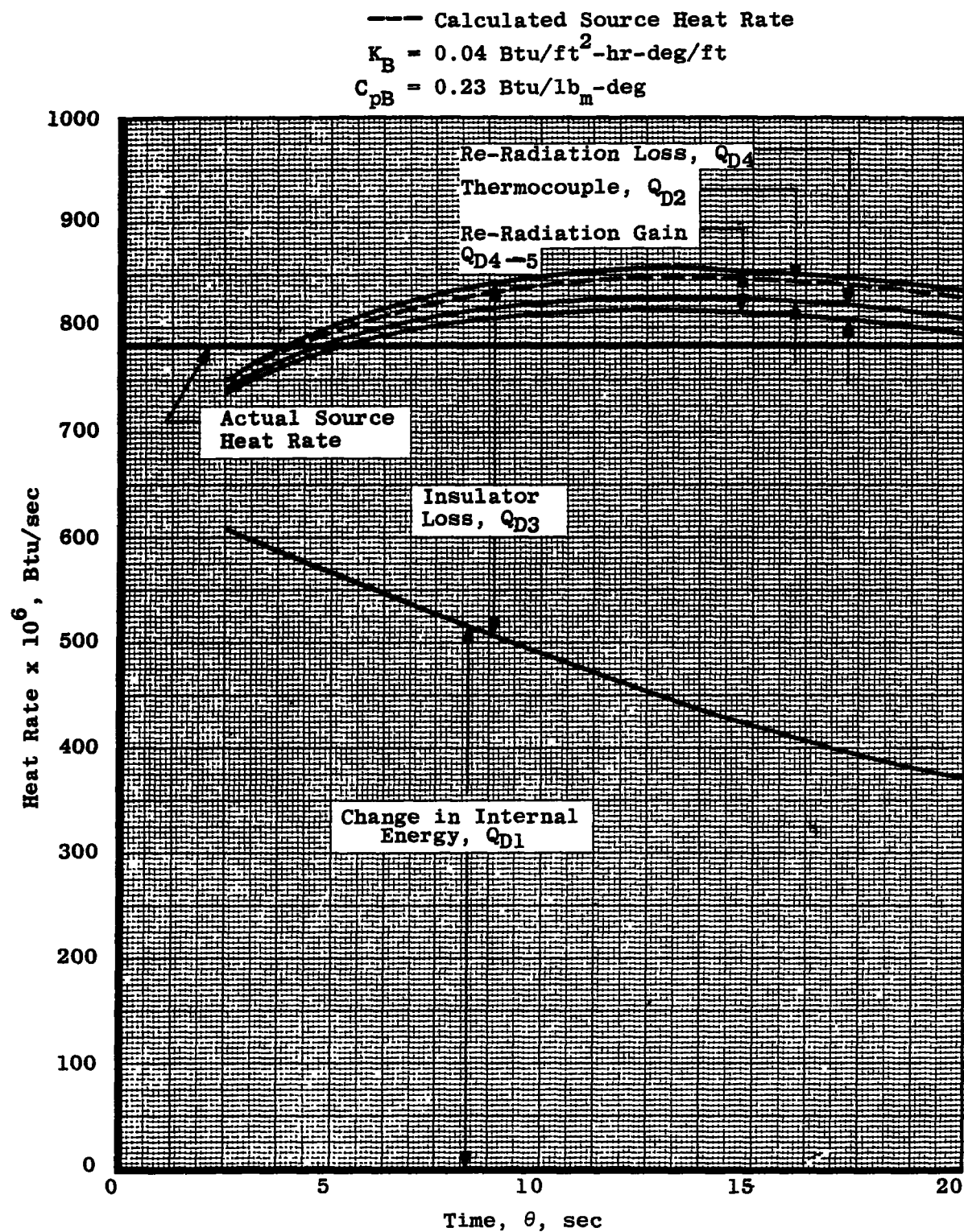
b. 0.15-in. Aperture

Fig. 16 Concluded



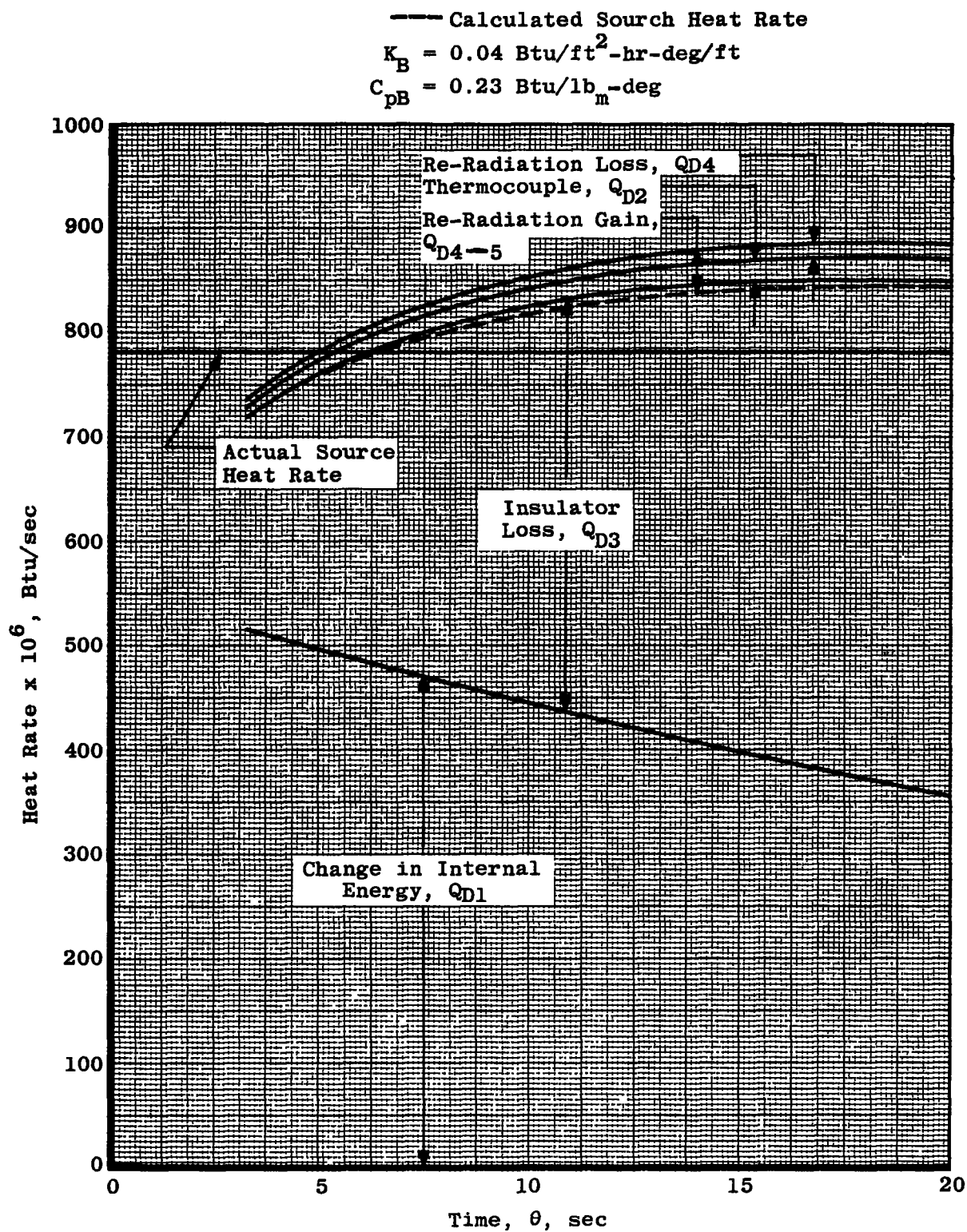
a. 0.05-in. Aperture (Time Zero at 3.75 sec)

Fig. 17 Black-Body Cavity Heat Rate-Time Histories



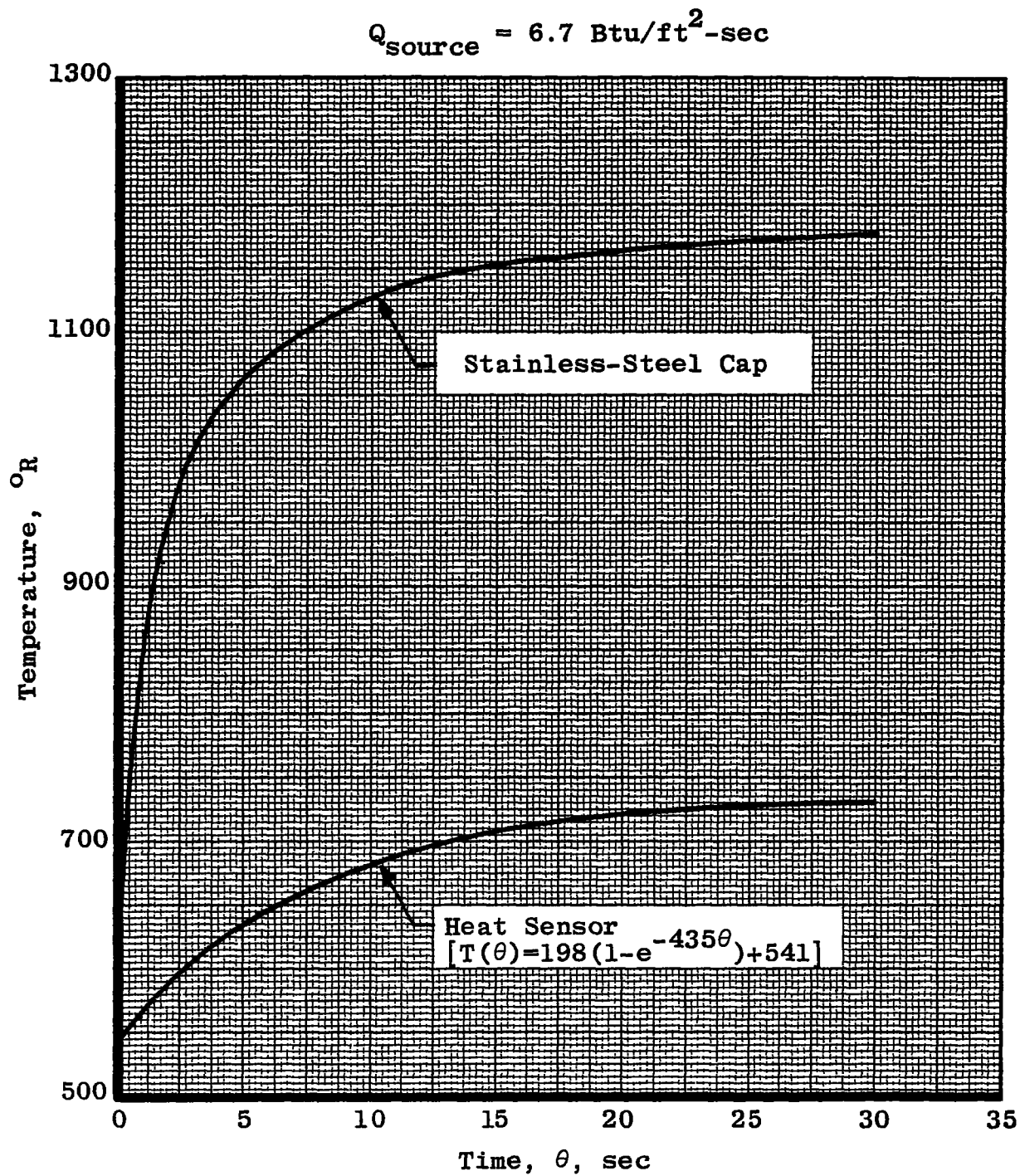
b. 0.15-in. Aperture (Time Zero at 2.5 sec)

Fig. 17 Continued



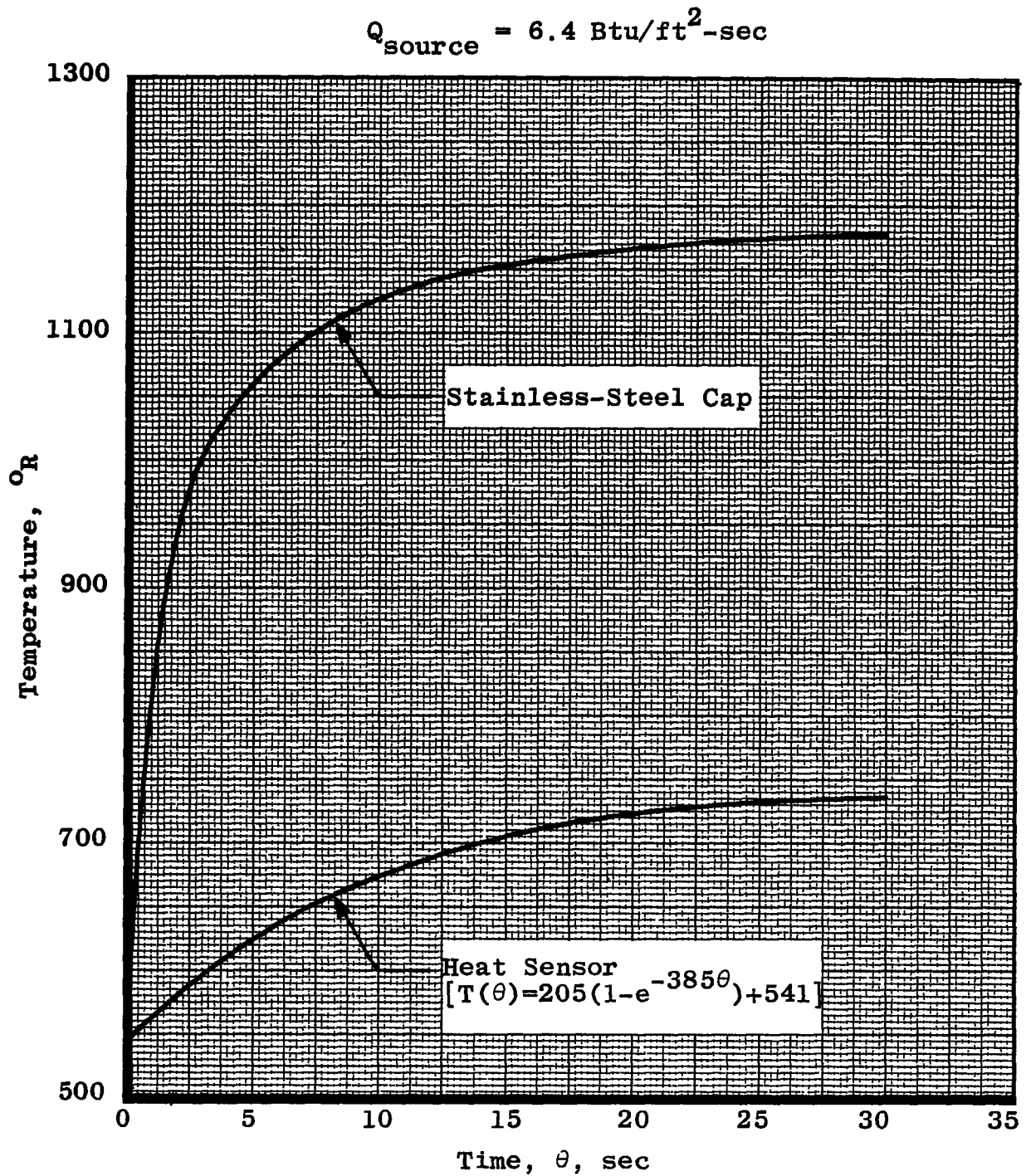
c. 0.15-in. Aperture (Time Zero at 1.25 sec)

Fig. 17 Concluded



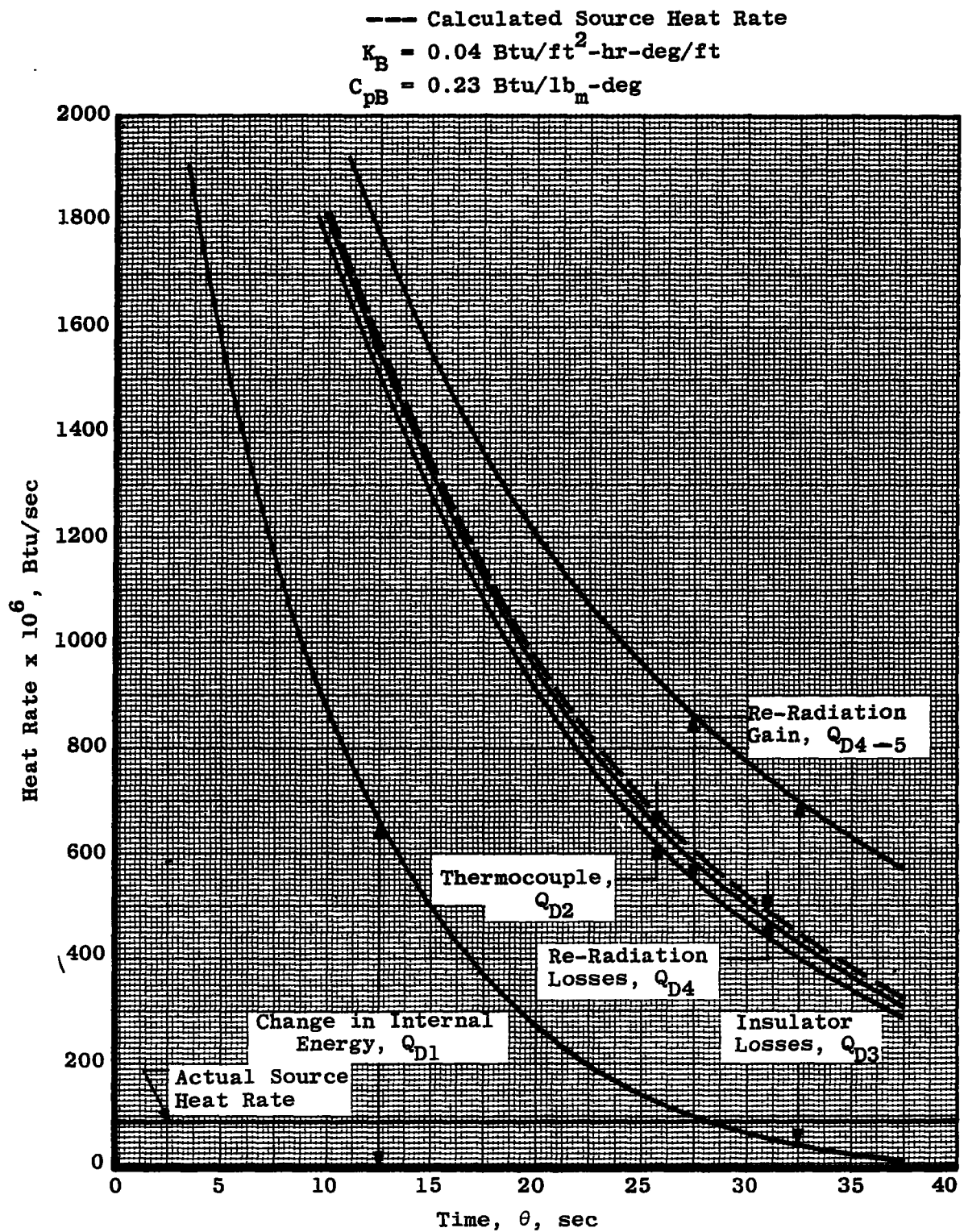
a. 0.05-in. Aperture

Fig. 18 Black-Body Cavity Temperature-Time Histories (External Convection)



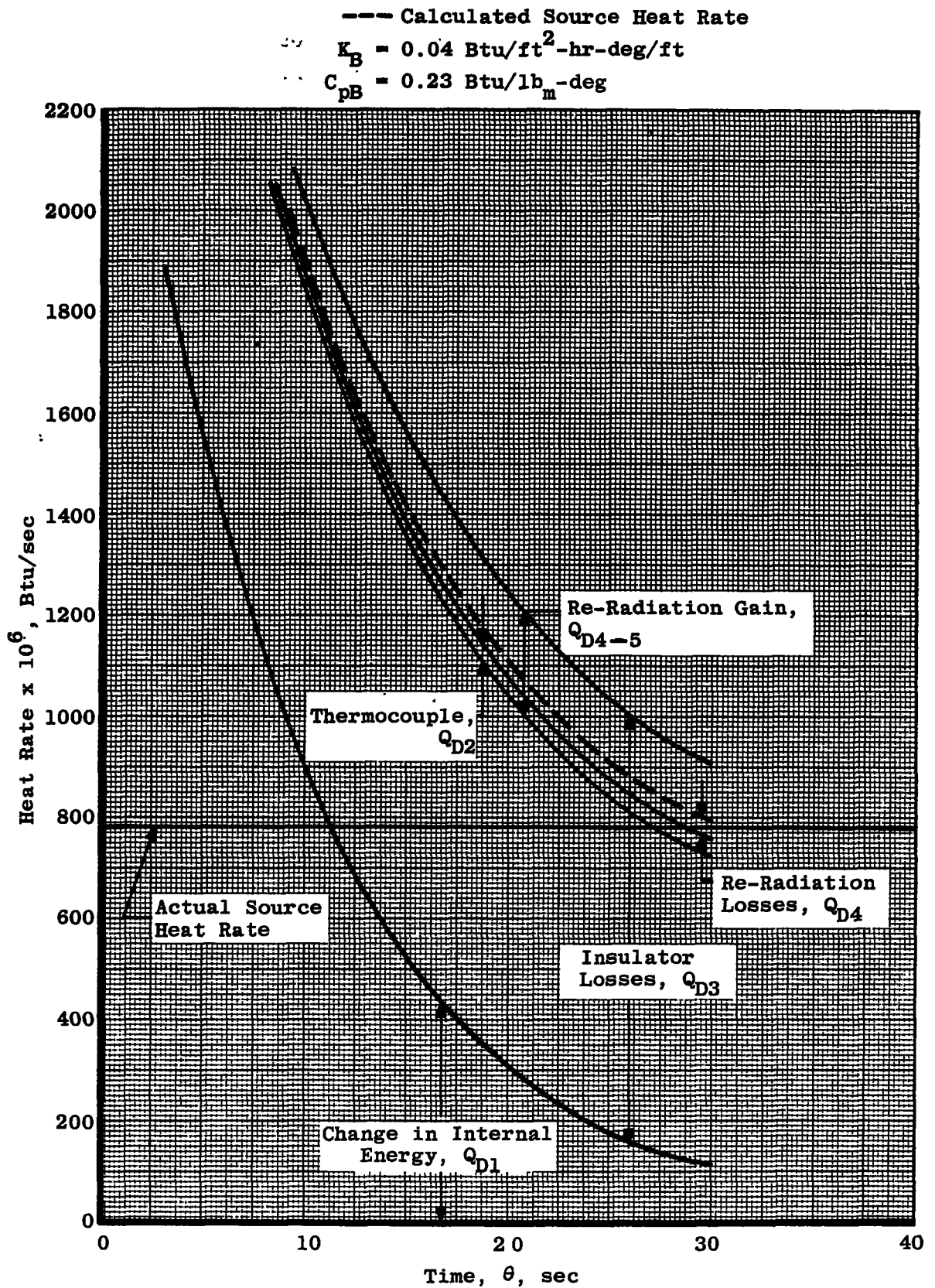
b. 0.15-in. Aperture

Fig. 18 Concluded



a. 0.05-in. Aperture

Fig. 19 Black-Body Cavity Heat Rate-Time Histories (External Convection)



b. 0.15-in. Aperture

Fig. 19 Concluded